

# Evaluation of Alpha-Synuclein and Tau Antiaggregation Activity of Urea and Thiourea-Based Small Molecules for Neurodegenerative Disease Therapeutics

Susantha K. Ganegamage, Taiwo A. Ademoye, Henika Patel, Heba Alnakhala, Arati Tripathi, Cuong Calvin Duc Nguyen, Khai Pham, Germán Plascencia-Villa, Xiongwei Zhu, George Perry, Shiliang Tian, Ulf Dettmer, Cristian Lasagna-Reeves, and Jessica S. Fortin\*

Cite This: *ACS Chem. Neurosci.* 2024, 15, 3915–3931

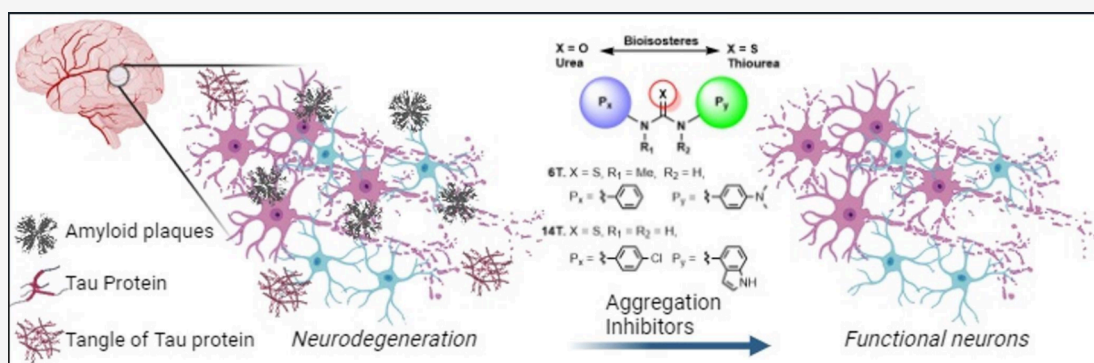
Read Online

ACCESS |

Metrics & More

Article Recommendations

Supporting Information



**ABSTRACT:** Alzheimer's disease (AD) and Parkinson's disease (PD) are multifactorial, chronic diseases involving neurodegeneration. According to recent studies, it is hypothesized that the intraneuronal and postsynaptic accumulation of misfolded proteins such as  $\alpha$ -synuclein ( $\alpha$ -syn) and tau, responsible for Lewy bodies (LB) and tangles, respectively, disrupts neuron functions. Considering the co-occurrence of  $\alpha$ -syn and tau inclusions in the brains of patients afflicted with subtypes of dementia and LB disorders, the discovery and development of small molecules for the inhibition of  $\alpha$ -syn and tau aggregation can be a potentially effective strategy to delay neurodegeneration. Urea is a chaotropic agent that alters protein solubilization and hydrophobic interactions and inhibits protein aggregation and precipitation. The presence of three hetero atoms (O/S and N) in proximity can coordinate with neutral, mono, or dianionic groups to form stable complexes in the biological system. Therefore, in this study, we evaluated urea and thiourea linkers with various substitutions on either side of the carbamide or thiocarbamide functionality to compare the aggregation inhibition of  $\alpha$ -syn and tau. A thioflavin-T (ThT) fluorescence assay was used to evaluate the level of fibril formation and monitor the anti-aggregation effect of the different compounds. We opted for transmission electron microscopy (TEM) as a direct means to confirm the anti-fibrillar effect. The oligomer formation was monitored via the photoinduced cross-linking of unmodified proteins (PICUP). The anti-inclusion and anti-seeding activities of the best compounds were evaluated using M17D intracellular inclusion and biosensor cell-based assays, respectively. Disaggregation experiments were performed with amyloid plaques extracted from AD brains. The analogues with indole, benzothiazole, or *N,N*-dimethylphenyl on one side with halo-substituted aromatic moieties had shown less than 15% cutoff fluorescence obtained with the ThT assay. Our lead molecules 6T and 14T reduced  $\alpha$ -syn oligomerization dose-dependently based on the PICUP assays but failed at inhibiting tau oligomer formation. The anti-inclusion effect of our lead compounds was confirmed using the M17D neuroblastoma cell model. Compounds 6T and 14T exhibited an anti-seeding effect on tau using biosensor cells. In contrast to the control, disaggregation experiments showed fewer A $\beta$  plaques with our lead molecules (compounds 6T and 14T). Pharmacokinetics (PK) mice studies demonstrated that these two thiourea-based small molecules have the potential to cross the blood–brain barrier in rodents. Urea and thiourea linkers could be

*continued...*

Received: May 4, 2024  
Revised: September 24, 2024  
Accepted: September 25, 2024  
Published: October 22, 2024



further improved for their PK parameters and studied for the anti-inclusion, anti-seeding, and disaggregation effects using transgenic mice models of neurodegenerative diseases.

**KEYWORDS:** Alzheimer's disease, anti-aggregation, neurodegeneration, Parkinson's disease, thiourea, urea

## INTRODUCTION

Alzheimer's disease (AD) is one of the most prevalent neurodegenerative diseases emanating from the misfolding of the two main prone-to-aggregate proteins. AD is characterized by the formation of extracellular plaques, intracellular neurofibrillary tangles (NFTs), drastic decline in acetylcholine levels in the brain, oxidative stress, and increased levels of misfolded proteins.<sup>1</sup> These perturbations aggravate several clinical manifestations, including loss of memory, decreased cognitive ability, and personality changes associated with AD. Extracellular plaques are deposits of amyloid- $\beta$  ( $A\beta$ ) proteins, having a variety of structural forms that include compact, classic, and diffuse plaques. The aggregation of these morphological forms of  $A\beta$  in the cerebral cortex of the brain usually results in microglia activation, which leads to neuroinflammation and axonal damage.<sup>2</sup> NFTs are formed from the disordered microtubule-associated protein tau (MAPT), otherwise known as the tau protein, and their accumulation in the neuron causes an impairment in the function and disassembly of the cytoskeletal microtubule.<sup>3</sup> Tau is predominantly located in neurons and its function mainly provides stability (through interaction with tubulin) to neuronal microtubules.<sup>4</sup> Tau is also essential for cell signaling.<sup>5</sup> The tau protein has six isoforms that are expressed in the brain of an adult, and they are generated through alternative splicing of the mRNA transcribed from the MAPT gene.<sup>6,7</sup>

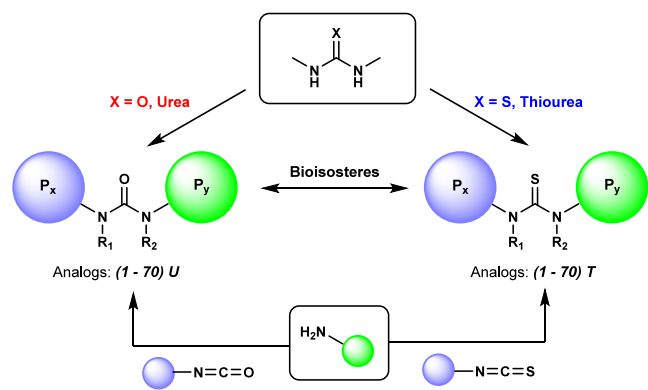
The tau protein is subjected to a variety of post-translational modifications. These modifications include glycation, ubiquitination, nitration, truncation, polyamination, and phosphorylation.<sup>8–10</sup> Tau proteins are more prone to phosphorylation than the other forms of modifications, and this creates the potential for excessive binding of the phosphoryl group to tau proteins, leading to hyperphosphorylation and a change of conformation resulting in fibrils.<sup>11</sup> If the tau protein is attached to microtubules, then hyperphosphorylation will cause it to dissociate from the microtubules, resulting in the formation of insoluble inclusions. NFTs are rich of misfolded hyperphosphorylated tau. According to one of the current hypotheses about AD pathophysiology, the aggregation of  $A\beta$  occurs early.  $A\beta$  plaques induce microglia activation, which enhances the hyperphosphorylation of tau and the formation of NFTs resulting in neurocognitive deterioration.<sup>12</sup> Hyperphosphorylation of tau, which is a promoter of neurocognitive deterioration, makes tau cytotoxic and more prone to aggregation.<sup>13</sup> Therefore, developing effective treatment models is crucial in inhibiting the spread of the disease. Most drugs developed for the treatment of AD are aimed only at managing symptoms and slowing the progression of the disease. These drugs exert their effect by either interfering with the conditions that promote the accumulation of  $A\beta$  and tau or raising the level of neurotransmitters in the brain to improve cognitive function. In recent times, efforts to understand the pathophysiology and the discovery of a drug for the treatment of AD have increased the awareness of the disease.<sup>14</sup>

AD includes the aggregation of  $A\beta$ , increased free radicals resulting from oxidative stress, poor neurotransmission, and microglial-mediated neuroinflammation. Some of the drugs developed to target these processes are directed toward  $A\beta$

clearance in the brain and are mainly  $\beta$ -secretase (BACE) inhibitors and acetylcholinesterase (AChE) inhibitors. Substantive efforts have been made in the development of therapeutics to treat AD. Some small molecule inhibitors developed to treat AD are designed for a single targeting role to either inhibit  $A\beta$  aggregation or tau fibrillization, but there has been limited patient efficacy.<sup>15</sup> Antibodies have also been developed with limited clinical benefits.<sup>16,17</sup> These failures in designing effective therapeutics are partly due to a lack of substantial knowledge in understanding the pathophysiological processes leading to the progression of AD and also failure to identify and optimize potential drug candidates to move past clinical trials.<sup>18</sup> Early diagnosis combined with the institution of multitarget approaches in pharmacotherapy, including altering the protein aggregation at the early stage, might be helpful in the clinical management of these chronic and devastating diseases.

To produce drug candidates with the anti- $\alpha$ -synuclein and anti-tau fibrillization potential for neurodegenerative diseases, our group has identified a family of compounds that can prevent fibril formation. In a previous study, our lab discovered the potential of phenylethylurea in preventing the fibrillization of islet amyloid polypeptide (IAPP).<sup>19</sup> Additional *in vitro* studies performed on  $\alpha$ -synuclein ( $\alpha$ -syn) indicated the importance of bisubstituted urea with an aromatic moiety for the fibrillization inhibition property. The best urea-based compound resulting from this study was composed of 5-aminoindole and 3,5-dichlorophenyl groups.<sup>20</sup> The scope of our work presented here is to explore the multitargeting role of urea and thiourea-linked compounds. Urea is a naturally occurring compound that is formed from the metabolism of proteins and nitrogen-containing compounds.<sup>20</sup> Ever since the original synthesis of urea and its analogue thiourea, these have been used for the development of several drugs because of the ability to improve the properties of drugs in terms of potency, selectivity, and activity.<sup>20</sup> One characteristic, unique to its function, is its ability to form a stable hydrogen bond with proteins, giving its biological activity as a precursor for the synthesis of various therapeutics. In this study, different aromatic moieties were attached to the urea/thiourea linker with one side (Py in Scheme 1) of the moieties being incorporated mainly with an indole, benzothiazole, aminofluorene, 4-morpholino, *N,N*-dimethylphenyl, and *p*-trifluoromethylphenyl. The selection of some of these substituents is based on their activity in stopping the formation of oligomers and fibrils as discovered previously from our group where we found both indole- and benzothiazole-based compounds to have a multitargeting effect on the aggregation of  $\alpha$ -syn and tau.<sup>21–23</sup> The nitrogen present in the urea/thiourea linker has been coupled with different substituents, including methyl, ethyl, and isopropyl, for effective structure–activity relationship determinations. The best compounds were further assessed with selected *in vitro* ADME assays and single-dose pharmacokinetics (PK) studies using CD1 mice, in addition to advanced characterization of their anti-oligomer, anti-inclusion, anti-seeding, and disaggregation effects.

**Scheme 1. Synthesis of Urea (U) and Thiourea (T) Analogues Using Respective Isocyanate and Isothiocyanate Reacting with Amines ( $R_1 = \text{H, Me, Et, or } i\text{-Pr}$  and  $R_2 = \text{H}$ )**



## RESULTS AND DISCUSSION

### Synthesis of Urea/Thiourea-Based Small Molecules.

The synthesis of comparable bioisosteric analogues of urea (denoted with the letter *U*) and thiourea (denoted with the letter *T*) is achieved through a reaction of the corresponding isocyanate or isothiocyanate with the respective amine via nucleophilic addition, as shown in Scheme 1. The reaction workup has been done with a simple crystallization with ethyl acetate–hexane to obtain a pure product with an acceptable yield ranging from 11 to 100% (Supporting Information, pages S2–S35).

Our previous findings demonstrated that ureas and indoles possess strong anti-aggregation activity. To validate our hypothesis, a variety of substituents were applied on one side of the urea/thiourea linker ( $P_x$  in Scheme 1), which consisted of phenyl, *p*-chlorophenyl, 3,5-dichlorophenyl, *p*-bromophenyl, *p*-iodophenyl, *p*-acetylphenyl, *p*-methylphenyl, 3-methylphenyl, 3,5-methylphenyl, *p*-methoxyphenyl, 3-thiomethylphenyl, *N,N*-dimethylphenyl, biphenyls, ethyl, and cyclohexyl. The aromatic moiety was sometimes distanced from the linker by a methyl, ethyl, or carbonyl moiety. In addition, different aromatic moieties were attached to the urea/thiourea linker on the other side ( $P_y$  in Scheme 1) of the molecules; the moieties being incorporated mainly consisted of an indole, benzothiazole, aminofluorene, 4-morpholino, *N,N*-dimethylphenyl, *p*-trifluoromethylphenyl, and cyclohexyl. The nitrogen present in the urea/thiourea linker has been coupled with different substituents, including methyl, ethyl, and isopropyl, in some instances (Table 1).

The kinetics of  $\alpha$ -syn fibril formation were assessed in the presence of a high micromolar concentration of urea/thiourea derivatives (Table 1). Due to the high number of compounds, a prescreening was performed using  $\alpha$ -syn at 2  $\mu\text{M}$ . For the selection of the best compounds, the cutoff was set using a maximum ThT fluorescence intensity below 15% after the subtraction of the standard error of the mean (SEM). It is challenging to inhibit the aggregation of prone-to-aggregate proteins. It is preferable to consider a very stringent cutoff to make sure that weak compounds are funneled down. For the compounds moving to advanced testing, assays were conducted using a higher concentration of proteins and a range of concentrations of compounds to assess dose–response. Compounds bearing an indole (compounds 10U, 14U, 14T, 15U, and 19U), benzothiazole (compound 16T), or *N,N*-dimethylphenyl (compound 6T) on one side with halo-

substituted aromatic moieties had shown less than 15% cutoff fluorescence obtained with the ThT assay and were then moved to advanced biophysical and biological testing. Compound 10U was not pursued for further testing due to the lack of substituents on the urea nitrogen and aromatic moiety. Compound 19U has been characterized extensively<sup>20</sup> and was only studied for PK using CD1 mice. As an interesting trend, the aminoindole small molecule derivatives were better to inhibit the  $\alpha$ -syn aggregation than the morpholino and aminofluorene analogues. Concerning the  $\alpha$ -syn anti-aggregation activity, inactive and very weak compounds contained these moieties among others: aliphatic, aromatic, biphenyl, and aminofluorene. An additional carbon between the aliphatic and urea or thiourea linkers reduced significantly the anti-aggregation activity. No other general trend could be drawn from the study, i.e., if the phenyl urea analogues exhibited superior anti-aggregation activities versus thiourea-based small molecules and vice versa (Table 1).

**ThT Anti-Fibrillization Kinetics.** The ThT assay serves as the first line of testing to evaluate the potential of synthesized compounds for their anti-fibril effect. This assay employs thioflavin T (ThT), which is a fluorescent dye that recognizes and binds to the  $\beta$ -pleated sheet structures of misfolded protein aggregates. Proteins that are susceptible to misfolding, such as tau and  $\alpha$ -syn, typically undergo a structural transformation from their native conformation to adopt a  $\beta$ -sheet structure when aggregated.<sup>24</sup> We screened our compounds for their anti-fibril effect on  $\alpha$ -syn and three isoforms of tau (0N3R, 2N3R, and 2N4R). Isoforms 4R and 3R are at equal concentrations in AD brains, which justify the utilization of those in a drug discovery program. The inhibition of aggregation is easier to obtain using short isoforms. Tangles are composed of a mixture of tau isoforms. Therefore, it is preferable to confirm the anti-aggregation effect utilizing several of these six isoforms. Compounds 6T and 14T showed the best anti-fibril action on  $\alpha$ -syn (Figure 1A), with compounds 14T and 19U having the lowest percentage (Table 1). The kinetics of aggregation of  $\alpha$ -syn is examined closely by utilizing a higher concentration to match the concentration used with the tau ThT assays. Interestingly, during the  $\alpha$ -syn aggregation kinetics (Figure 1A), a delay in the lag time (time for the elevation in fluorescence intensity) is present following treatment with 14T and 6T, indicative of inhibition of oligomer formation. Compound 19U has been extensively studied prior to this work and was only used in the mice study.<sup>20</sup> Prism analysis yielded a LogEC50 of  $29.8 \pm 3.7$  for compound 14T in the correlation between Log (agonist) and the normalized response (variable slope) (Figure 1B). To explore the dual target ability of the compounds, we tested them for their tau anti-fibril effects. The first of the tau series was the 0N3R isoform, where only compounds 6T and 14T were tested, and compound 14T was deemed the best, having a 66% reduction in fibril formation versus 7% for compound 6T after 18 h of incubation (Figure 2A). In addition to evaluating compounds 6T and 14T, we further examined additional sets of compounds (38T and 18T) on tau 2N3R. At the conclusion of the experiment, it was observed that virtually all the compounds effectively halted tau 2N3R fibrillization (Figure 2B). The compounds demonstrated a significant reduction in tau 2N3R, with the following order of efficacy: 18T (97%), 6T (96%), 14T (79%), and 38T (70%). As for tau 2N4R, we observed a decrease of 34 and 67% for 6T and 14T, respectively (Figure 2B).

**PICUP Assay Assessment of the Anti-Oligomer Effect of Compounds.** The photoinduced cross-linking of unmodi-

**Table 1. Maximum Thioflavin-T (ThT) Fluorescence Intensity in Percentage (%) Resulting from the Plateau Phase of the Kinetics of  $\alpha$ -Syn Aggregation with the Presence of DMSO and Diaryl Derivatives of Urea and Thiourea<sup>a</sup>**

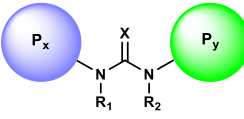
Analog Number	Functional Groups					
	P <sub>x</sub>	P <sub>y</sub>	Substitutions		X = O, Urea (U)	X = S, Thiourea (T)
			R <sub>1</sub>	R <sub>2</sub>	Maximum ThT fluorescence intensity (%) ± SEM	Maximum ThT fluorescence intensity (%) ± SEM
01			H	H	>100	>100
02			Me	H	>100	>100
03			Et	H	>100	>100
04			<i>i</i> -Pr	H	>100	>100
05			H	H	47 ± 6	43 ± 1
06			Me	H	38 ± 8	17 ± 3
07			Et	H	35 ± 3	53 ± 1
08			<i>i</i> -Pr	H	36 ± 3	44 ± 9
09			H	H	99 ± 2	95 ± 8
10			H	H	10 ± 2	55 ± 1
11			H	H	71 ± 3*	81 ± 4
12			H	H	66 ± 8	91 ± 5
13			H	H	56 ± 3	74 ± 9
14			H	H	15 ± 3**	8 ± 1
15			H	H	14 ± 3	59 ± 10
16			H	H	>100	13 ± 1
17			H	H	99 ± 7*	92 ± 15
18			H	H	>100	19 ± 2
19			H	H	6 ± 2**	49 ± 3
20			H	H	84 ± 4	>100
21			H	H	>100	>100
22			H	H	>100	61 ± 12
23			H	H	35 ± 3	52 ± 4
24			H	H	29 ± 3**	66 ± 8
25			H	H	95 ± 3	74 ± 8



Table 1. continued

26			H	H	88 ± 2	90 ± 7
27			H	H	94 ± 4	88 ± 7
28			H	H	20 ± 4	25 ± 1
29			H	H	35 ± 11	45 ± 2
30			H	H	24 ± 2	64 ± 1
31			H	H	46 ± 1	52 ± 1
32			H	H	43 ± 3	64 ± 3
33			H	H	>100	>100
34			H	H	78 ± 2	68 ± 1
35			H	H	79 ± 4	>100
36			H	H	60 ± 5	51 ± 4
37			H	H	33 ± 4	81 ± 18
38			H	H	25 ± 4	25 ± 2
39			H	H	83 ± 13	49 ± 7
40			H	H	27 ± 7	45 ± 6
41			H	H	38 ± 1	38 ± 4
42			H	H	43 ± 3	24 ± 1
43			H	H	64 ± 10	41 ± 15
44			H	H	46 ± 1	46 ± 1
45			H	H	69 ± 3	57 ± 2
46			H	H	32 ± 2**	90 ± 5
47			H	H	51 ± 6**	91 ± 2
48			H	H	76 ± 7**	68 ± 1
49			H	H	>100	>100

Table 1. continued

50			H	H	19 ± 1	23 ± 3
51			H	H	50 ± 2	26 ± 1
52			H	H	18 ± 1	28 ± 1
53			H	H	58 ± 1	71 ± 11
54			H	H	73 ± 5	56 ± 3
55			H	H	67 ± 4	63 ± 2
56			H	H	88 ± 12***	59 ± 4
57			H	H	84 ± 2	>100
58			H	H	64 ± 5	68 ± 5
59			H	H	89 ± 1	90 ± 2
60			H	H	76 ± 3	82 ± 1
61			H	H	82 ± 4	40 ± 2
62			H	H	67 ± 4	57 ± 20
63			H	H	46 ± 3	49 ± 7
64			H	H	63 ± 3	69 ± 1
65			H	H	61 ± 2	95 ± 15
66			H	H	73 ± 2	72 ± 7
67			H	H	45 ± 3	71 ± 8
68			H	H	81 ± 2	>100
69			H	H	41 ± 9	87 ± 10
70			H	H	90 ± 7	93 ± 1

<sup>a</sup>Data are presented as the mean of three replicates ± the SEM. The fluorescence intensity of  $\alpha$ -syn with the vehicle (DMSO) was set at 100%. A total of 140 molecules were tested at 100  $\mu$ M, and the anti-fibrillary effect was evaluated with  $\alpha$ -syn at 2  $\mu$ M. Molecules resulting in a maximum fluorescence intensity of 15% by subtracting the SEM (as indicated in red) were subjected to additional biophysical analyses. Among the 140 small molecules prepared in this study, 9 of them have been already published by our research group in the following journal articles: \*Fortin et al. in J. Mol. Struct. 1267 (2022) 133574;<sup>18</sup> \*\*Maity et al. in J. Mol. Struct. 1249 (2022) 13156; and<sup>20</sup> \*\*\*Fortin et al. in Can. J. Physiol. Pharmacol. 94 (2016) 341.<sup>19</sup>

fied proteins (PICUP) assay utilizes the action of Tris(2,2'-bipyridyl)ruthenium(II) chloride (Ru(bpy)<sup>3</sup>) and ammonium persulfate (APS), which are electron- and radical-generating compounds, respectively, to induce oligomer formation. This photochemical assay has been utilized to examine the impact of

compounds on the formation of oligomers, which are the initial events preceding fibril formation. PICUP assays with  $\alpha$ -syn cannot be achieved at a concentration lower than 30  $\mu$ M with our experimental settings. Various concentrations of compounds were tested, and the desirable effect should occur at a

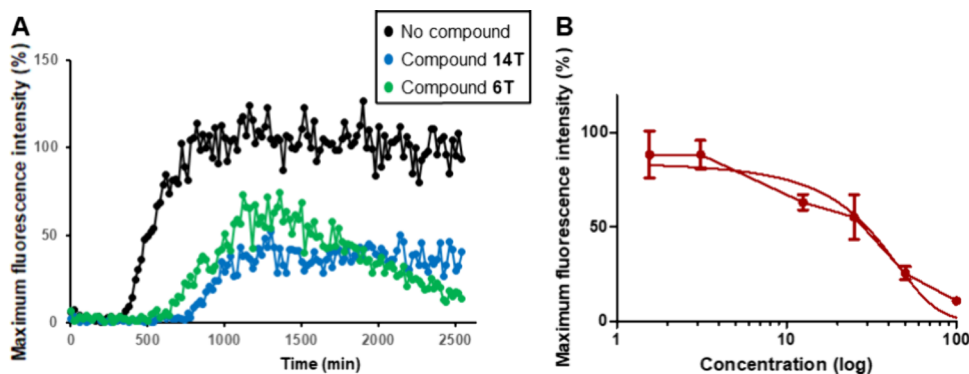


**Figure 1.** Kinetics of  $\alpha$ -syn aggregation showed a delay in the lag time (time for the elevation in fluorescence intensity) in the presence of compounds 14T and 6T, indicative of inhibition of oligomer formation. Compound 14T inhibited the  $\alpha$ -syn aggregation in a dose-dependent manner. The ThT fluorescence assay was employed to analyze the kinetic curves of compounds 14T and 6T at a concentration of 100  $\mu$ M with (A)  $\alpha$ -syn (6  $\mu$ M) and (B) compound 14T dose-dependent inhibition at varying concentrations (3.125, 6.25, 12.5, 25, 50, and 100  $\mu$ M) against  $\alpha$ -syn (6  $\mu$ M) fibril formation. Data were collected in triplicate for each concentration at the plateau phase over the course of five consecutive time points. The error bars indicate the SEM for each condition.

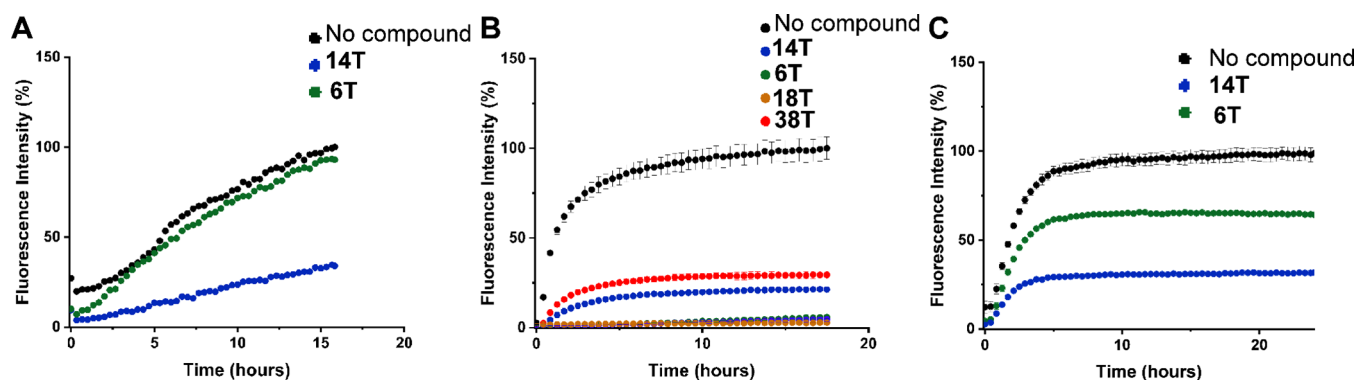


**Figure 2.** ThT kinetic curve showing the effect of the best anti-fibrillary compound (14T and 6T) when assessed with different tau isoforms. The compounds were tested at a concentration of 100  $\mu$ M along with 10  $\mu$ M (10:1), including (A) tau 0N3R, (B) tau 2N3R, and (C) tau 2N4R. Several compounds were tested for their anti-fibrillary effect on tau 2N3R. The best anti-fibrillary compounds were 14T and 6T when assessed with tau 0N3R and 2N4R. The kinetics were performed in the presence of 2.5  $\mu$ M heparin, 1 mM dithiothreitol (DTT), 1 mM 4-(2-aminoethyl) benzenesulfonyl fluoride hydrochloride, and 30  $\mu$ M ThT in a buffer solution containing 50 mM Tris and 25 mM NaCl, at pH 7.4. The positive control was the tau isoform without compound treatment. The background (BG) signal was obtained with all components in the absence of tau proteins and compounds. The depicted curves represent the average data obtained from three technical replicates.

lower molar ratio. Compounds that showed an anti-fibrillization effect from the ThT experiment with a cutoff below 15% (including the subtraction of the SEM) were selected for the PICUP assay, i.e., compounds 6T, 14U, 14T, 15U, and 16T. Oligomer (around 37–40 kDa) formed from  $\alpha$ -syn monomers is represented in Figure 3. Compared to the control, compounds 6T and 14T prevented the formation of oligomers. Compounds 14U and 15U did not inhibit oligomerization. Among the promising compounds, 14T and 6T were the most effective. Compounds 14T and 16T were further tested to determine whether they have a dose-dependent effect. The compounds proved to be effective from 12.5 to 50  $\mu$ M (Figure 4). Our previous work and the analysis herein indicate that the urea compounds with indole and aromatic-*N*-methyl are most likely to inhibit  $\alpha$ -syn oligomers. The anti-oligomer effect detected with PICUP assays herein correlates with the lag time delay observed in Figure 1A.

The effect of compounds 14T and 6T was assessed in a dose-dependent manner at different concentrations (50, 100, and 200  $\mu$ M) on the oligomerization of tau 0N4R and 2N4R isoforms. Across the tested concentrations, compound 14T showed no effect on stopping the formation of both tau 0N4R and tau

2N4R oligomers (Figures 5 and 6). A similar result was observed for the effect of compound 6T on tau 2N4R (Figure 6). However, at 100 and 200  $\mu$ M, compound 6T slightly reduced oligomerization of tau 0N4R (Figure 5). The prospect of the anti-oligomer effect of compound 6T was further explored on tau 0N3R. When compared to the control with no compound treatment, compound 6T showed a minimal effect on stopping tau 0N3R oligomerization (Figure 7). The anti-oligomerization of tau is challenging and depends on the isoform tested. Compound 6T demonstrated a minimal degree of anti-oligomerization with the shorter isoforms of tau.

**Direct Visualization of Fibril Formation.** For the validation of the anti-fibrillar effect of compounds 6T and 14T (the best inhibitors), transmission electron microscopy (TEM) was used as a direct method to identify both  $\alpha$ -syn and tau 2N4R fibrils. After the completion of the  $\alpha$ -syn ThT assay measuring the kinetics of aggregation at low concentrations of the protein (i.e., 2  $\mu$ M), samples were obtained to examine fibrils and assess the effect of the best compounds (100  $\mu$ M of 6T and 14T) in comparison to the control (DMSO). This is regularly done as quality control to confirm the validity of the ThT assay. Both compounds significantly reduced  $\alpha$ -syn fibrillization (Figure 8)

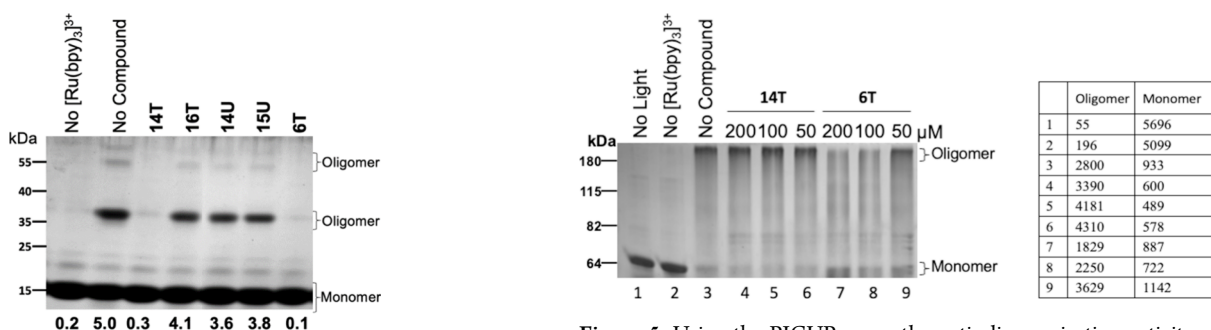


**Figure 3.** Compounds **6T** and **14T** stopped the formation of  $\alpha$ -syn-induced oligomer formation resulting from the exposure of Tris(2,2'-bipyridyl)ruthenium(II) chloride ( $\text{Ru}(\text{bpy})_3^{3+}$ ) and APS to light (1 s) through the PICUP cross-linking assay. At  $60 \mu\text{M}$ ,  $\alpha$ -syn was subjected to cross-linking (PICUP assay) with **6T**, **14U**, **14T**, **15U**, and **16T** at  $100 \mu\text{M}$ . Compounds **6T** and **14T** effectively prevented the formation of oligomers observed between 35 and 40 kDa. The high molecular weight  $\alpha$ -syn oligomer was observed in the Coomassie blue-stained polyacrylamide gels with the control (0.125% DMSO). Other controls include no light and no cross-linking agent ( $\text{Ru}(\text{bpy})_3^{3+}$ ), which yielded no cross-linked products. The numbers indicated below the gels represent the ratio of the oligomer and monomer. The pixel density of bands was acquired by using ImageJ software.

**Figure 5.** Using the PICUP assay, the anti-oligomerization activity of the most promising compounds against tau ON4R was evaluated in a dose–response manner. In this assay, compounds **14T** and **6T** at varying concentrations, 50, 100, and  $200 \mu\text{M}$ , were incubated with the protein ( $12 \mu\text{M}$ ). Bands indicating higher molecular weights appeared in the control condition, which lacked both light exposure and the cross-linking agent,  $\text{Ru}(\text{bpy})_3^{3+}$ . The anti-oligomer effect was observed for compound **6T** at  $100 \mu\text{M}$  and  $200 \mu\text{M}$ . The pixel density of monomer and oligomer bands presented in the table was measured for each lane using ImageJ.

after visualization at 40k magnification. Compounds **6T** and **14T** were further evaluated at 6 or 12.5, 25, and  $100 \mu\text{M}$  to determine their dose–response effect using a higher concen-

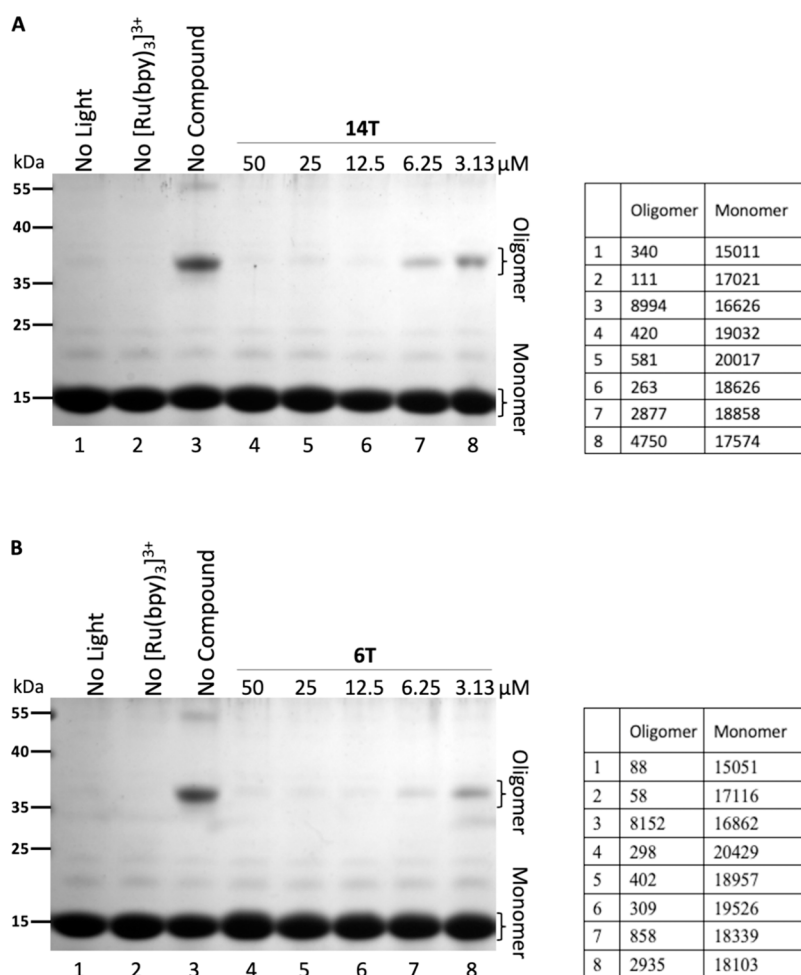


**Figure 4.** Dosage-dependent ability of compounds (A) **14T** and (B) **6T** to inhibit  $\alpha$ -syn oligomerization. In the oligomer induction experiment,  $\alpha$ -syn ( $60 \mu\text{M}$ ) was cross-linked with different concentrations (50, 25, 12.5, 6.25, and  $3.13 \mu\text{M}$ ) of compounds **14T** and **6T**. Both compounds showed a dose-dependent ability to stop the oligomerization of  $\alpha$ -syn. The control consisted of DMSO (0.125%). The pixel density of monomer and oligomer bands presented in the table was measured for each lane using ImageJ.



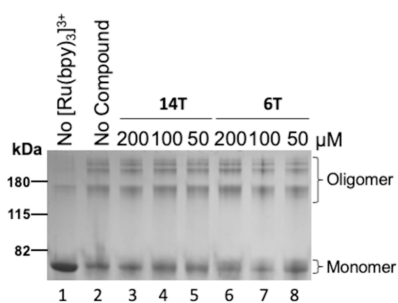


**Figure 6.** Dose-dependent inhibitory effect of compounds **14T** and **6T** on tau 2N4R ( $6 \mu\text{M}$ ) oligomerization via PICUP. Both compounds did not demonstrate dose-dependent inhibition of tau 2N4R oligomerization. The control conditions (no compound treatment and  $\text{Ru}(\text{bpy})_3^3$ ) exhibited high molecular weight tau 2N4R oligomers.

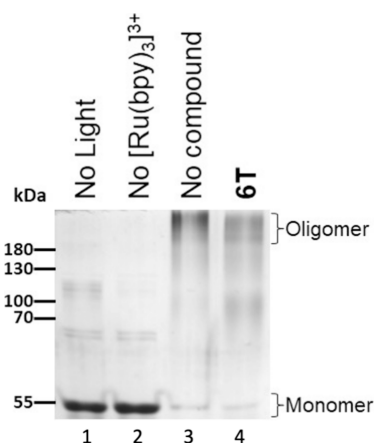


**Figure 7.** Effectiveness of compound **6T** ( $50 \mu\text{M}$ ) in preventing tau ON3R oligomerization was tested at  $10 \mu\text{M}$  through the PICUP assay. The control groups that did not contain  $\text{Ru}(\text{bpy})_3^3$  and had no light exposure showed no higher molecular weights.

tration of  $\alpha\text{-syn}$  (i.e.,  $6 \mu\text{M}$  as depicted in ThT dose–response in Figure 1B), and it was observed that its greatest effect occurred at a concentration of  $100 \mu\text{M}$  (Figure 9).

TEM analyses were performed on tau 2N4R from a commercial source (rPeptide, Watkinsville, GA, USA) and homemade in the lab. Compounds **6T** and **14T** were evaluated at  $100 \mu\text{M}$ . After incubation for 24 h at  $37^\circ\text{C}$ ,  $6 \mu\text{M}$  tau 2N4R

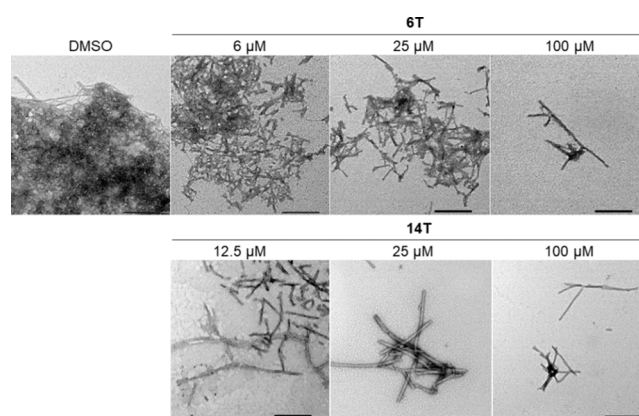


**Figure 9.** TEM evaluation of the dose-dependent effect of compounds **6T** and **14T** on preventing the formation of  $\alpha\text{-syn}$  mature fibrils. The protein  $\alpha\text{-syn}$  ( $6 \mu\text{M}$ ) was exposed to DMSO (0.25%; “CTRL”), and the compounds were tested at 6.25 or 12.5, 25, and  $100 \mu\text{M}$ . The samples were left to incubate for approximately 22 h at  $37^\circ\text{C}$  before being visualized. Scale bars represent 200 nm.

from the commercial source resulted in multifocal packets of intertwined fibrils, sometimes in row and chain conformations after incubation. Compound **14T** resulted in fewer fibrils with a shorter appearance. Compound **6T** had a minimal impact on the reduction of tau 2N4R fibril formation. TEM analyses of the reaction solution extracted at the end of the ThT assays, as shown in Figure 2C, were performed with the homemade tau 2N4R at  $10 \mu\text{M}$ . The fibrils obtained from the kinetics are individualized and elongated (Figure 10). A similar trend was observed from the two compounds after treatment. Compound **14T** resulted in the formation of short and less dense 2N4R fibrils when compared to the control (Figure 10). On the opposite, compound **6T** failed to reduce the density of fibrils.

Circular dichroism (CD) was used with  $\alpha\text{-syn}$  to confirm the change in the secondary structure induced by the best compound. Compound **14T** was subjected to this additional analysis because of its effect in preventing the  $\alpha\text{-syn}$  inclusion in neuroblastoma cell (please see the results in Figure 15). CD spectra of  $\alpha\text{-syn}$  incubated at different time points in the absence (control: 0.25% DMSO) and presence of compound **14T** are shown in Figure 11. The CD spectra of  $\alpha\text{-syn}$  alone (control) are characteristic of unfolded, random coils at time 0 h. Without any

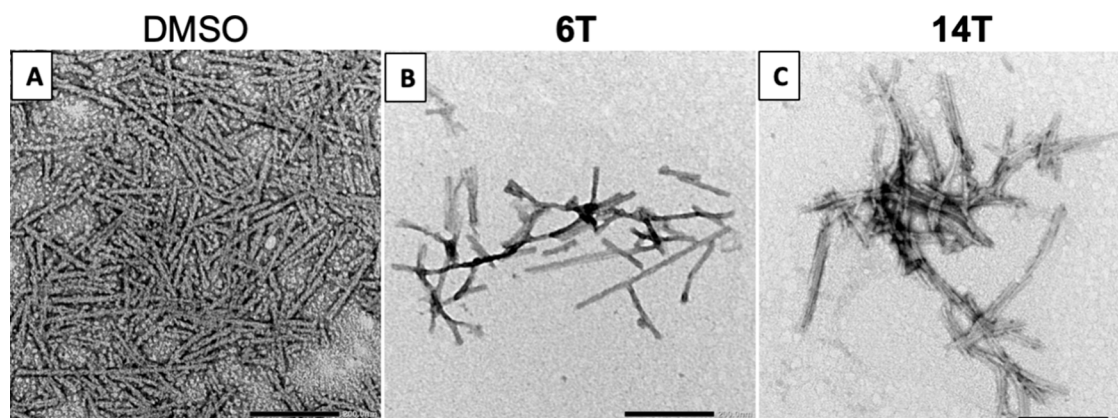


**Figure 8.** Effect of compounds **6T** and **14T** on preventing the formation of  $\alpha\text{-syn}$  mature fibrils was examined by TEM. (A)  $\alpha\text{-Syn}$  ( $2 \mu\text{M}$ ) was exposed to DMSO (0.25%; “CTRL”). (B)  $\alpha\text{-Syn}$  ( $2 \mu\text{M}$ ) received treatment with compound **6T** at  $100 \mu\text{M}$ . (C)  $\alpha\text{-Syn}$  ( $2 \mu\text{M}$ ) underwent treatment with compound **14T** at  $100 \mu\text{M}$ . All samples were incubated for approximately 22 h before TEM visualization. Scale bars represent 200 nm.

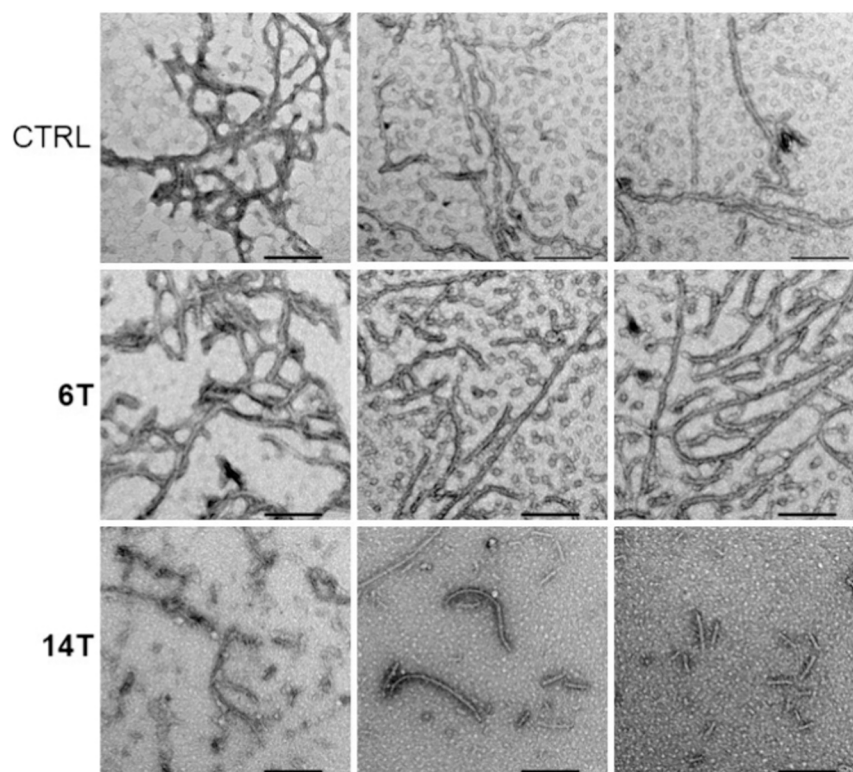


**Figure 10.** Treatment with compounds **6T** and **14T** led to a reduction in tau 2N4R ( $10\ \mu\text{M}$ ) fibrils, as observed through TEM. Unfolded tau 2N4R was incubated with DMSO at 0.25% (CTRL, control), compound **6T** at  $100\ \mu\text{M}$ , and compound **14T** at  $100\ \mu\text{M}$ . TEM images were taken at 40k magnification. Scale bars represent 200 nm.

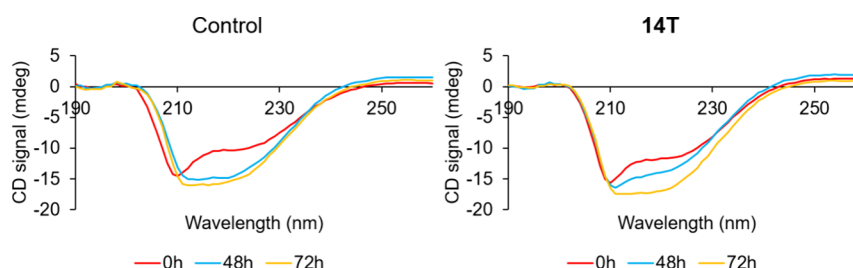


**Figure 11.** Compound **14T** delayed the conversion of  $\alpha$ -syn into the beta-sheet conformation at 48 h by CD analysis. CD spectra were recorded to provide structural information after the treatment of  $\alpha$ -syn (at  $15\ \mu\text{M}$ ) with 0.25% DMSO (control) or  $100\ \mu\text{M}$  compounds **14T** for 0, 48, and 72 h. The buffer consisted of 10 mM PBS supplemented with 0.5 mM SDS and 300 mM NaCl. Samples were incubated for 48 and 72 h at  $37\ ^\circ\text{C}$  before the analysis. CD spectra were recorded. The BG signal (buffer alone) was subtracted.

inhibitor of aggregation, there is a clear conversion of the  $\alpha$ -syn random coil conformation into the  $\alpha$ -helix and beta-sheet conformation at 48 and 72 h. The treatment with  $100\ \mu\text{M}$  of compound **14T** resulted in a delay of this conversion. In contact with compound **14T**, the  $\alpha$ -syn protein remained in a random coil with the mixture of  $\alpha$ -helix/beta-sheet conformations at 48 h and the transition into beta-sheet conformations occurred at 72 h (Figure 11). The peak at 225 nm corresponds to a beta-sheet conformation at 72 h.

**Disaggregation of  $A\beta$  Plaques Isolated from AD Patients.** The multitarget effect of compounds **6T** and **14T** was further explored to determine if the compounds had a disaggregation potential on  $A\beta$  plaques isolated from AD patients. Samples were obtained from the brain of an AD patient and subsequently treated with compounds **6T** and **14T** at  $50\ \mu\text{M}$ . TEM micrographs for  $A\beta$  plaques were taken at 2500, 20k, and 40k magnifications. The 2500 $\times$  magnification demonstrates the plaque-like materials present after the incubation with

different treatments (Figure 12). The 20k magnification vividly shows the compact arrangement (density) of the formed fibrils, while the 40k magnification helps to distinguish the changes in the fibrillar structures postcompound treatment. In comparison to the control (0.25% DMSO), the micrographs demonstrated the disaggregation effects resulting from compounds **6T** and **14T** (predominantly **6T**) on the  $A\beta$  plaques extracted from AD brains (Figure 12).

To confirm that the disaggregation activity of compounds does not generate high molecular weight species (toxic oligomers), incubation of preformed  $\alpha$ -syn fibrils was done followed by electrophoresis and Western blot analysis. Compound **6T** was tested due to its predominant disaggregation activity with the AD plaques. Disaggregation experiments were performed with  $60\ \mu\text{M}$   $\alpha$ -syn fibrils in 10 mM PBS supplemented with 0.5 mM SDS and 300 mM NaCl. Compound **6T** was tested at  $200\ \mu\text{M}$  for 4 days at  $37\ ^\circ\text{C}$ . The compound did not generate more oligomers in comparison with



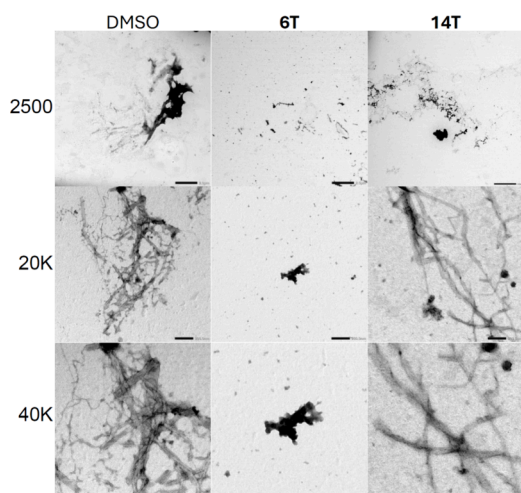


**Figure 12.** Compound 6T demonstrated a reduction in A $\beta$  plaques, as confirmed through TEM. A $\beta$  ( $0.217 \pm 0.042$  mg/mL) obtained from the brain of an AD patient underwent incubation with DMSO (0.25%; referred to as control), compound 6T (at  $50 \mu\text{M}$ ), or compound 14T (at  $50 \mu\text{M}$ ) for 5 days before TEM visualization. Scale bars represent 200 nm.

the control (DMSO). The antibody used for the Western blot, shown in Figure 13 (anti-alpha-synuclein 33), detected the oligomers located between 35 and 40 kDa. The oligomers are less present with the mature fibrils treated with compound 6T.

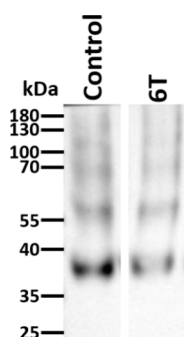


**Figure 13.** Compound 6T reduced the formation of oligomer following the disaggregation experiment performed with  $\alpha$ -syn fibrils. Mature  $\alpha$ -syn fibrils were incubated with  $100 \mu\text{M}$  compound 6T for 4 days at  $37^\circ\text{C}$  and then loaded in 16% SDS–PAGE gel. The Western blot was assessed using anti-alpha-syn 33 to recognize the oligomers (bands higher than 35 kDa). The control consisted of the vehicle (0.25% DMSO).

The results presented on the anti-aggregation and disaggregation activity of compounds 6T and 14T are suggestive of a general mechanism. Due to the broad activity on several prone-to-aggregate proteins, these compounds most likely recognize a general common structure. One of the mechanisms of action suspected is that these compounds are disruptors of a beta-pleated sheet.

**$\alpha$ -Syn Inclusion-Forming Neuroblastoma Cell Assay.** M17D neuroblastoma cells expressing the fusion protein  $\alpha\text{S-3K::YFP}$  were utilized to assess the impact of compounds 6T and 14T on both cell viability and inclusion formation. The presence of the triple K mutations ( $\alpha\text{S E35K + E46K + E61K (=}\alpha\text{S3K)$ ) “amplifies” the  $\alpha\text{S}$  missense mutation E46K found in familial PD patients.<sup>25–27</sup>  $\alpha\text{S3K}$  mutations make the protein,  $\alpha$ -

syn, readily prone to form round cytoplasmic inclusions in the cell system utilized, herein M17D neuroblastoma cells. These cells expressing  $\alpha\text{S3K}$  have delayed growth and exhibit cell stress and toxicity.<sup>28</sup> Several compounds were capable of reducing the formation of the  $\alpha\text{S}$  inclusions<sup>18,20,22,23,29,30</sup> and  $\alpha\text{S}$ -induced cytotoxicity.<sup>28</sup> The neuroblastoma cells utilized in this assay expressed an  $\alpha\text{S-3K::YFP}$  fusion protein in a doxycycline (dox)-inducible-dependent manner. The induction caused pronounced round YFP-positive inclusions in the cells treated with the vehicle (DMSO) in the absence of a compound (Figure 14A,B). Compounds 14U, 15U, and 16T exhibited anti-fibrillary activity below 15% but were unable to reduce the oligomer formation. These compounds were used as negative controls and did not exhibit a substantial anti-inclusion activity below a concentration of  $40 \mu\text{M}$  (Figure 14).

Compounds 6T and 14T have been identified for their anti-fibril and anti-oligomer abilities using ThT and PICUP assays. Using the  $\alpha$ -syn inclusion-forming neuroblastoma assay, compound 14T exhibited a significant reduction in the formation of inclusions (Figure 15). Compound 14T had a greater effect at 2.5, 5, 10, and 20, while compound 6T showed the most significant effect (although weak) at  $40 \mu\text{M}$ . The two compounds did not show any effect on the confluency of the cells.

**Anti-Seeding Effect of Compounds 14T and 6T in TauRD P301S FRET Biosensor Cells.** Using the TauRD P301S FRET biosensor model, we next looked at whether compounds 6T and 14T reduced tau seeding. The cell-based experiment entails the production of tau seeds and the treatment of biosensor cells with the seeds. The production of tau seeds is achieved by the expression of htauP301S in vitro. Human embryonic kidney (HEK) 293T cells were transfected with the htauP301S plasmid to overexpress human P301S tau. The compounds (14T and 6T) or the vehicle (control, 0.01% DMSO) was applied to HEK 293T cells post 24 h of transfection. Following 48 h of exposure to the compounds at 5 and  $20 \mu\text{M}$  doses, cell viability and tau seeding activity were evaluated (Figure 16A). HEK 293T cell viability was not impacted by treatment with the vehicle (0.01% DMSO) or compounds 14T and 6T (Figure 16B). Cell lysates from P301S tau overexpressing cells treated with compounds 14T and 6T exhibited reduced seeding activity compared to lysates from cells treated with the vehicle (0.01% DMSO) alone (Figure 16C,D).

**In Vitro ADME Testing: Solubility and Microsomal Stability.** The MSU Medicinal Chemistry Core facility conducted kinetic solubility assessments for the most promising compounds, as detailed in Table 2. Compared to the  $100 \mu\text{M}$  concentration used in the ThT assay (all within the same buffer solution), compound 6T has a solubility greater than 100 and even  $300 \mu\text{M}$ , and compound 14T has a solubility greater than  $100 \mu\text{M}$ . This indicates a notable disparity in solubility between the two compounds, with compound 6T showcasing considerably higher solubility compared to compound 14T. For the advanced testing, compounds 6T and 14T were tested using the concentration within the range of solubility. The anti-fibrillization effect observed with compounds 6T and 14T is independent of the solubility.

In the mouse microsomal stability assay (Table 3), the control (imipramine) has a retention capacity of 44% of its initial amount after 30 min. When compared to the control, compound 6T demonstrates a higher value of 74% indicating potentially higher stability while compound 14T exhibits a lower

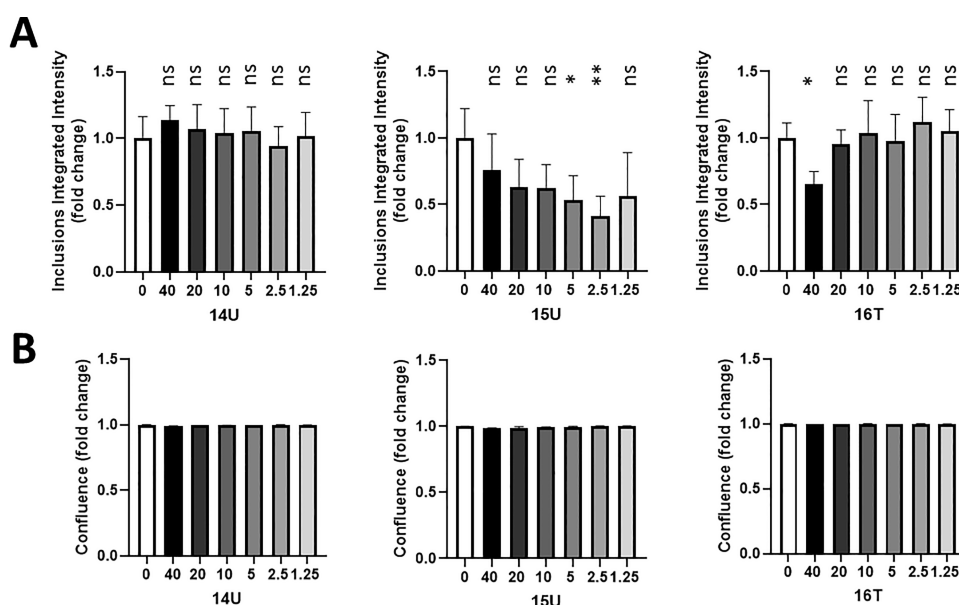


**Figure 14.** Compounds 14U, 15U, and 16T did not prevent substantially  $\alpha$ -syn inclusion formation at a low micromolar concentration. (A) M17D cells expressing the inclusion-prone  $\alpha$ S-3K::YFP fusion protein (dox-inducible) were treated with 0.1% DMSO (vehicle; “0  $\mu\text{M}$ ”) as well as 1.25, 2.5, 5, 10, 20, and 40  $\mu\text{M}$  of compounds 14U, 15U, and 16T at  $t = 24$  h after plating. Cells were induced with dox at  $t = 48$  h. Incucyte-based analysis of punctate YFP signals relative to 0.1% DMSO was done at  $t = 96$  h ( $N = 2$  independent experiments,  $n = 6$ –12 individual wells total 0  $\mu\text{M}$ ,  $n = 12$ ; 40, 20, and 10  $\mu\text{M}$ ,  $n = 6$ ; all other concentrations,  $n = 12$ ). (B) Plot of confluence fold changes relative to the DMSO vehicle (0  $\mu\text{M}$ ). All data are presented as fold changes relative to DMSO control  $\pm$  standard deviation. One-way ANOVA, Dunnett’s post hoc test; \* $p < 0.05$ ; \*\* $p < 0.01$ ; \*\*\* $p < 0.001$ ; \*\*\*\* $p < 0.0001$ ; ns, non-significant.

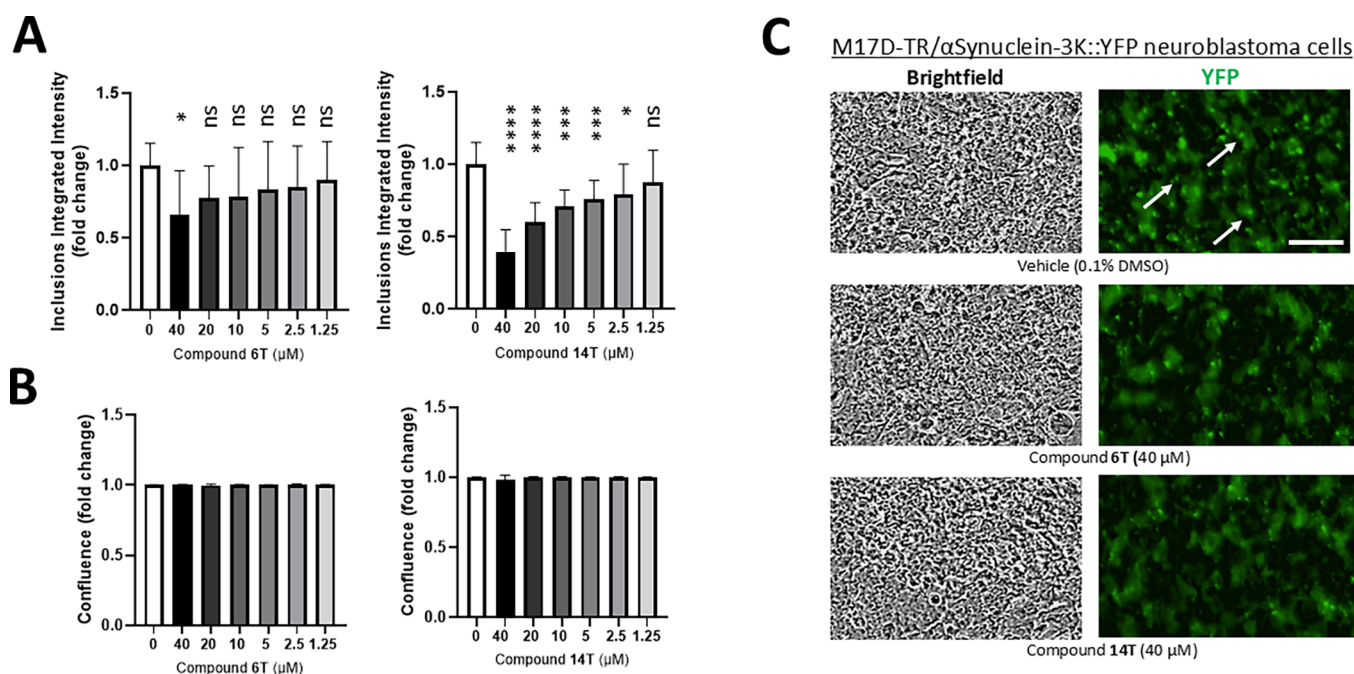


**Figure 15.** Compound 14T mainly prevents  $\alpha$ -syn inclusion formation. M17D cells expressing the inclusion-prone  $\alpha$ S-3K::YFP fusion protein (dox-inducible) were treated with 0.1% DMSO (vehicle; “0  $\mu\text{M}$ ”) as well as 1.25, 2.5, 5, 10, 20, and 40  $\mu\text{M}$  of compounds 6T and 14T at  $t = 24$  h after plating. Cells were induced with dox at  $t = 48$  h. (A) Incucyte-based analysis of punctate YFP signals relative to 0.1% DMSO was done at  $t = 96$  h in  $N = 4$  (compound 6T) or  $N = 3$  (compound 14T) independent experiments,  $n = 9$ –24 individual wells total. For compound 6T: 0  $\mu\text{M}$ ,  $n = 18$ ; 40, 20, and 10  $\mu\text{M}$ ,  $n = 9$ ; all other concentrations,  $n = 18$ . For compound 14T: 0  $\mu\text{M}$ ,  $n = 24$ ; 40, 20, and 10  $\mu\text{M}$ ,  $n = 11$ ; all other concentrations,  $n = 24$ . (B) Same as panel (A), but confluence fold changes relative to the DMSO vehicle (0  $\mu\text{M}$ ) were plotted. (C) Representative Incucyte images of reporter cells treated with the vehicle vs 40  $\mu\text{M}$  compounds 6T and 14T ( $t = 96$  h), phase and green channel. Arrows indicate  $\alpha$ S-rich and YFP-positive inclusions. Scale bar represents 50  $\mu\text{M}$ . All data are presented as fold changes relative to DMSO control  $\pm$  standard deviation. Kruskal–Wallis tests plus Dunn’s multiple comparisons test; \* $p < 0.05$ ; \*\*\* $p < 0.001$ ; \*\*\*\* $p < 0.0001$ , ns, non-significant.

percentage remaining at 25%, suggesting it might be more prone to degradation.

**Single-Dose PK.** The PK study for the best drug candidate was carried out by Pharmaron, China, using a CD1 male mouse



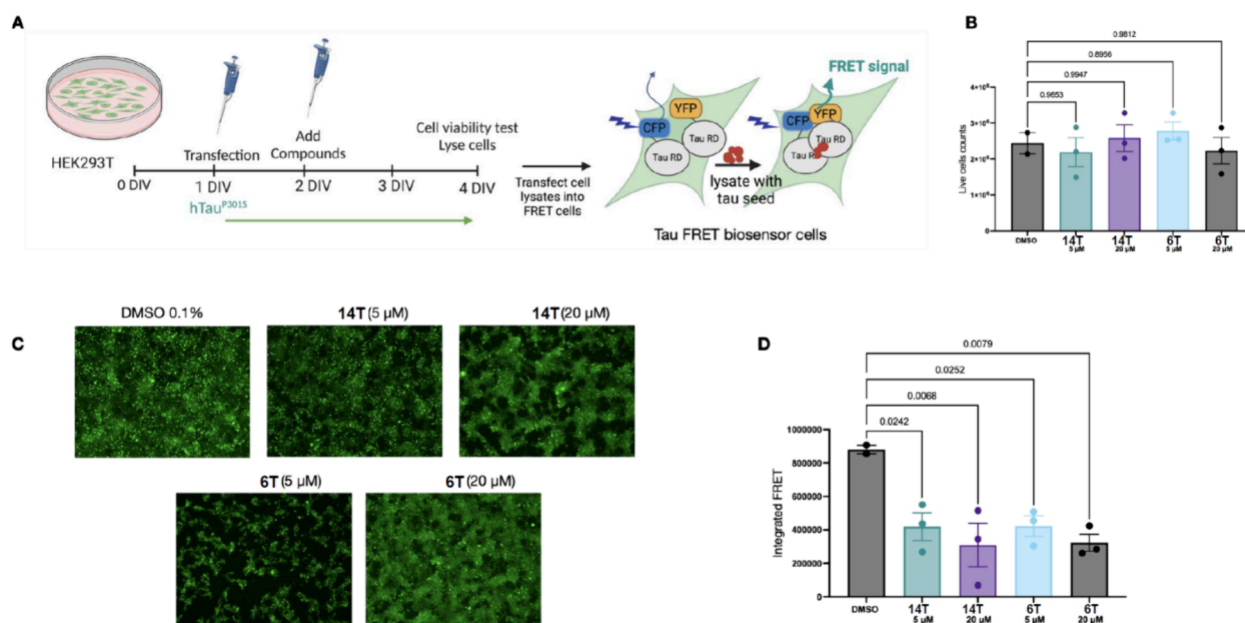


**Figure 16.** Compounds 6T and 14T reduce the tau seeding activity in vitro. (A) Schematic of the experimental setup to test the effect of compounds on tau seeding activity. The htauP301S plasmid was transfected to overexpress tau in HEK 293T cells, and the cells were treated with the compounds 24 h later. Cell viability and tau seeding activity were assessed 48 h after treatment with compounds. (B) Viability of HEK cells after treatment with the compounds. The compound treatments in HEK 293T were performed in 3 biological replicates ( $N = 3$  per condition). (C) Representative images of the FRET signal from biosensor cells after transfection with HEK cell lysates. (D) Seeding activity of cells overexpressing htauP301S and after treatment with the compounds. Values are given as the means  $\pm$  SEM of two technical replicates of the  $N = 3$  treated HEK 293T cells (B). Significance was determined by unpaired one-way analysis of variance (ANOVA).

**Table 2. Kinetic Solubility of Compounds 6T and 14T<sup>a</sup>**

compound	measured solubility ( $\mu\text{M}$ )
6T	>100
14T	>100
mebendazole	40

<sup>a</sup>Kinetic solubility of compounds. Compounds 6T and 14T (best compounds) were solubilized in ThT buffer composed of 10 mM PBS (pH = 7.4) with an additional 300 mM NaCl and 0.5 mM SDS. A final concentration of DMSO consisted of 1%. Mebendazole was used as a standard.

**Table 3. Microsomal Stability of Compounds 6T and 14T<sup>a</sup>**

compound	mouse microsome (% remaining at 30 min)
6T	74
14T	25
imipramine	44

<sup>a</sup>The experiment involves using a test compound at a concentration of 3  $\mu\text{M}$ , with four replicates conducted to ensure reliability and consistency of results. The solution comprises 100 mM phosphate buffer (pH 7.4), 3 mM  $\text{MgCl}_2$ , NADPH (cofactor) at a concentration of 1 mM, and 1% DMSO. Mouse microsomes were set at 0.25 mg/mL. At a specific time point of 30 min, the stability of the test compound was assessed using LC-MS/MS analysis and the % remaining was recorded.

and single intravenous administration (Figure 17). The PK studies were performed to determine the potential of the best compounds to cross the blood–brain barrier. In addition to the best compounds found herein, compound 19U, previously characterized *in vitro*, was included in the PK study due to its excellent  $\alpha$ -syn anti-oligomer, anti-fibril, and anti-inclusion activities.<sup>20</sup> Compounds 6T, 14T, and 19U resulted in a plasma:brain ratio  $\geq 1$ , which supports that these compounds

cross the blood–brain barrier. When compared to 14T, compounds 19U and 6T exhibited an increased exposure and a larger volume of distribution in the plasma, suggesting superior pharmacokinetic characteristics. A small amount of the compound was administered, which may have resulted in a short half-life. However, microsomal stability is below 70% for compound 14T, which may indicate the involvement of phase 1 metabolism. Optimization of compounds will address the microsomal stability issues in future studies.

## CONCLUSIONS

We examined the anti-aggregation effect of 140 small molecules containing a urea/thiourea linkage, with either an indole or phenyl benzothiazole analogue, against the aggregation of  $\alpha$ -syn. Analysis of  $\alpha$ -syn ThT fluorescence reveals that the compounds exhibiting indole or  $N,N$ -dimethylphenyl on one end, along with halo-substituted aromatic groups on the other, emerge as the most efficacious inhibitors of fibril formation. The most promising compounds were examined for their ability to inhibit both anti-oligomer and anti-fibrillar activities on different tau isoforms. Compound 6T emerged as the best inhibitor of tau 0N4R oligomerization. Compounds 6T and 14T both showed great effects against 2N3R (ThT assay) and 2N4R (TEM) fibrillization. Also, 6T was the best in disaggregating the A $\beta$  plaques. Compound 14T showed notable effectiveness in reducing the A $\beta$  plaques and the number of M17D  $\alpha$ -syn inclusions. Both compounds 6T and 14T reduced the level of seeding of htauP301S in biosensor cells and crossed the blood–brain barrier in CD1 mice. Mechanistic studies will confirm the hypothesis of these compounds being most likely beta-sheet breakers in future studies. Additionally, optimization will be performed to improve pharmacokinetic properties in rodents, i.e. metabolic stability and half-life.

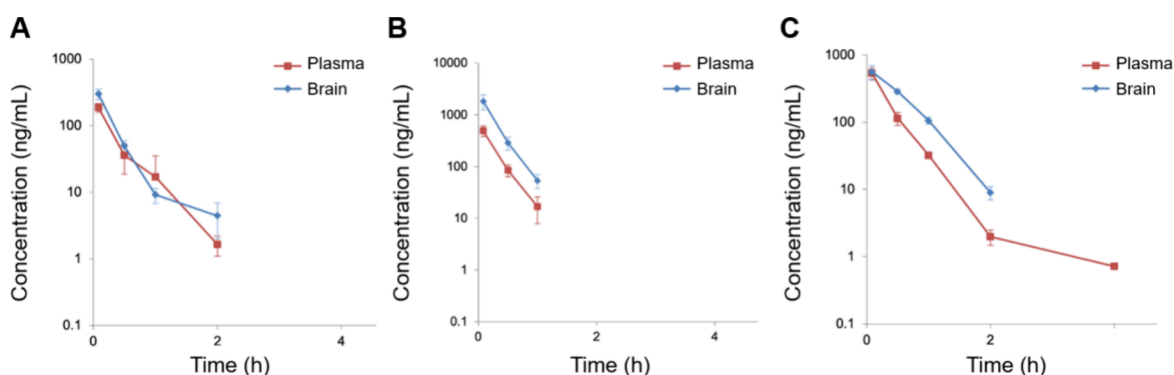


**Figure 17.** Mean plasma and brain concentration–time curve of compounds (A) 6T, (B) 14T, and (C) 19U in CD1 male mouse after intravenous administration of 1 mg/kg. Data are expressed as mean with the standard deviation.

## METHODS

**Chemical Synthesis. General Information.** The urea and thiourea derivatives were prepared with the nucleophilic addition of commercial anilines and isocyanates or isothiocyanates as published previously.<sup>18,20,21</sup> Detailed chemical characterization can be found in the Supporting Information.

**Biophysical Methods. ThT Kinetic Assay.** The thioflavin fluorescence assay is an established technique used to study the action of compounds in interfering with fibril formation. Previous studies have examined the fibril formation kinetics of recombinant  $\alpha$ -syn.<sup>18,23,30</sup> A stock solution of 277  $\mu$ M  $\alpha$ -syn was prepared by dissolving the protein (obtained from r-peptide) in 20 mM Tris–HCl (pH 7.4). The resulting solution was then diluted in ThT buffer (10 mM PBS buffer (pH 7.4), 0.5 mM SDS, and 300 mM NaCl). ThT and compounds at a final concentration of 40 and 100  $\mu$ M were first added to a 96-well transparent flat bottom plate (nontreated). Diluted  $\alpha$ -syn was then added, with each well having a total volume of 150  $\mu$ L to have the final concentration of  $\alpha$ -syn at 2  $\mu$ M. The BG signal was generated using a solution composed of ThT, buffer, and 0.25% DMSO. Conversely, the positive control included  $\alpha$ -syn, along with ThT, buffer, and 0.25% DMSO.

We further examined the effect of the best compounds on tau isoforms 0N3R, 2N3R, and 2N4R. Regarding this, tau at a final concentration of 10  $\mu$ M was diluted in CHELEX-treated buffer containing 50 mM Tris and 25 mM NaCl (pH 7.4) and then supplemented with 100  $\mu$ M compound, 30  $\mu$ M ThT, 1 mM DTT, 2.5  $\mu$ M heparin, and 1 mM of 4-(2-aminoethyl)benzenesulfonyl fluoride hydrochloride at an overall volume of 200  $\mu$ L/well in a 96-well plate. Untreated tau serves as a positive control. All components were used without the addition of protein to acquire the BG signal. The BioTek Synergy plate reader was used to generate the ThT fluorescent signal for both tau 2N3R and  $\alpha$ -syn. The plate was incubated at 37 °C while being shaken at 200 rpm at regular intervals, and fluorescence readings were taken every 5 min. The data generated were plotted using the BioTek Gen5 software, and the excitation and emission wavelengths were 440 and 480 nm, respectively. To ensure the reliability of the data, the measurements were carried out in triplicate and repeated multiple times using different stock solutions of both proteins.

**Chemical and Protein (Peptide) Source.** ThT for  $\alpha$ -syn ThT assays was acquired from Alfa Aesar (Ward Hill, MA), and for tau 0N3R ThT assays, it was purchased from Sigma-Aldrich (St. Louis, MO). Millipore-Sigma supplied the heparin sodium salt, and recombinant  $\alpha$ -syn and tau 2N4R were procured from rPeptide (Watkinsville, GA). For tau 0N4R, a bacterial expression plasmid including the vector pET30a bearing a cDNA encoding the human tau 0N4R isoform was kindly provided by Dr. Benjamin Wolozin (Boston, MA) for expression and purification. The Rosetta BL21 E. coli (CamR) stock, which contains pET30a[0N4R tau wt] (KanR), was cultured in the LB medium supplemented with 50  $\mu$ g/mL of kanamycin and 50  $\mu$ g/mL of chloramphenicol. One mM IPTG was added to the culture, and cells were incubated for around 18 h at 37 °C to promote protein overexpression; thereafter, cells were centrifuged at 6000g for 15 min at

4 °C to extract the pellets. Pellets were suspended in the lysis solution (10 mM Hepes pH 7.4, 50 mM NaCl, 1 mM MgCl<sub>2</sub>, 1 mM PMSF, 1× PIC, 0.5 mM DTT), and the cells were lysed by sonication for about 3–5 m at 30 s on, 1 min off, and between 30 and 45% power. The supernatant was transferred with 7.8 mL (total) of 3 M NaCl after the lysate was centrifuged at 10,000 g for 10 min at 4 °C. After 10 min of incubation in a water bath at 80 °C, the lysate was cooled in an ice bath for a further 10 min. The lysate was then centrifuged for 10 min at 10,000 g and 4 °C, and the supernatant was transferred to fresh tubes. The supernatant was dialyzed overnight against a cation exchange buffer (pH 6.0, including 50 mM MES, 1 M NaCl, and 1 mM DTT). A linear gradient ranging from 50 mM to 1 M NaCl was used to elute the proteins from the dialysate after it was put onto a HiPrep SP HP column. After fractions that contained tau isoform 0N4R, the protein solution was dialyzed against PBS (pH 7.4) and kept at –80 °C.

**0N3R, 2N3R, and 2N4R Expression and Purification.** The method previously described for all three tau isoforms was used for their expression and purification.<sup>31–33</sup> Following transformation, BL21 (DE3) was produced from the pET-47b(+) vector carrying the 0N3R or 2N3R gene and the pET-14b vector carrying 2N4R. The fantastic broth medium was inoculated with an overnight-grown starter culture and cultivated at 37 °C with 200 rpm of shaking. 0.1 mM IPTG was used for 3–6 h at 37 °C to produce protein overexpression at an OD<sub>600</sub> of 0.6–0.8. The expressing cells were again suspended in the lysis buffer (pH 7.4), which contains 25 mM Na<sub>3</sub>PO<sub>4</sub>, 300 mM NaCl, 5 mM imidazole, 1 mM DTT, and 1 mM PMSF. Via sonication, reconstituted cells were lysed for 10 min at 60% power, with 30 s of on and 10 s of off. The cell lysate was centrifuged at 100,000 g. Ni-NTA was used to purify tau from the supernatant. Imidazole was eliminated by dialyzing the Ni-NTA elute. Human rhinovirus (HRV) 3C protease was then used to cleave off the His-tag by incubating it with tau at a 1:100 molar ratio for 4 h at 4 °C. His-tag-free tau was then isolated using a second Ni-NTA column. Before any additional processing, the Ni-NTA fraction containing His-tag-free tau was dialyzed against a salt-free buffer before purification. Using 50 mM Tris at pH 7.4 and 50 mM Tris, 1 M NaCl at pH 7.4 as Buffers A and B, respectively, tau was purified using a HiTrap SP Sepharose FF cation exchange column. Using a PD10 desalting column, fractions containing tau were buffer exchanged into 50 mM Tris, 25 mM NaCl, pH 7.4, and kept at –80 °C until needed. One gram of CHELEX beads per one liter of buffer was added to each buffer in this phase and left overnight.

**PICUP Assay.** The formation of  $\alpha$ -syn and tau oligomers was induced by cross-linking. The stock solution of  $\alpha$ -syn was diluted in PBS to obtain a final concentration of 60  $\mu$ M. Tau (all isoforms) was diluted to achieve a concentration of 6  $\mu$ M. Two  $\mu$ L of Tris(2,2'-bipyridyl)-ruthenium(II) chloride (Ru(bpy)<sub>3</sub>) complex, serving as a photosensitizer, was added at a final concentration of 300  $\mu$ M. The compounds to be tested were first diluted from a stock of 40 mM in DMSO to obtain a working concentration of 400  $\mu$ M in PBS, and the final concentrations that were used were based on the experiment setup. Two  $\mu$ L of APS was added to complement the action of the Ru(bpy)<sub>3</sub> complex, and the resulting mixture (a total volume of 20  $\mu$ L) was

exposed to light in order to induce the cross-linking of the protein monomers. The controls include samples that have not been exposed to light, did not contain Ru(bpy)<sup>3</sup> or APS, and did not include any compound (i.e., 0.125% DMSO). Both APS and Ru(bpy)<sup>3</sup> were added to the sample mixture before the light exposure. For  $\alpha$ -syn, the exposure time was 1 s, while the tau isoforms have a 60 s exposure time. Light exposition was achieved using a 53 W (120 V) glowing filament lamp in a custom-built dark box. The radical reaction was terminated with the addition of 8.3  $\mu$ L of Laemmli loading buffer containing 15%  $\beta$ -mercaptoethanol, followed by an incubation period of 10 min at 95 °C. Tau and  $\alpha$ -syn samples were loaded on a 16% SDS–PAGE gel and then visualized following Coomassie blue staining.

**TEM.** TEM was used to detect the formation of fibrils after the completion of the ThT kinetics of fibril formation. Ten  $\mu$ L of each sample (tau,  $\alpha$ -syn, and A $\beta$ ) was loaded onto a 400-mesh Formvar carbon-coated copper grid (Electron Microscopy Sciences, Hatfield, PA) in preparation for the EM analysis. The grid with the samples was incubated for 1 min, followed by three successive rinses with distilled water. The samples were carefully air-dried before being incubated for 1 min in a freshly prepared 1% uranyl acetate solution. Excess liquid was absorbed from the grid with filter paper and then air-dried. The grids were analyzed by using a JEOL 1400 Flash (from Japan) transmission electron microscope. Micrographs were captured at 40-fold magnification and an acceleration voltage of 100 kV.

**CD.** CD spectra were recorded at 25 °C under a constant flow of N<sub>2</sub> using a JASCO-810 spectropolarimeter (Jasco, Easton, MD). The instrument was set with a wavelength range of 180–250 nm. Measurements were acquired using a quartz cuvette of 1 mm path length and an instrument scanning speed of 100 nm/min, with a response time of 2 s and a bandwidth of 1 nm. All  $\alpha$ -syn samples were prepared using a final concentration of 15  $\mu$ M in 10 mM PBS buffer (pH 7.4) containing 300 mM NaCl and 0.5 mM SDS. Prior to measurement, samples were incubated at 37 °C for 0, 48, and 72 h. 0.25% DMSO with the buffer alone (no  $\alpha$ -syn) was used as the baseline and subtracted from subsequent readings of all samples. Each result is given as the average of 5 scans taken of three measurements at room temperature.

**$\alpha$ -Syn Inclusion-Forming Neuroblastoma Cell Experiment.** A previous study has performed this assay using the dox-induced M17D-TR/ $\alpha$ S-3K::YFP neuroblastoma cells.<sup>28</sup> A 96-well plate was used for the cell plating at a density of 30,000 cells/well. After 24 h of cell plating, the tested compounds were added, and the induction of  $\alpha$ S-3K::YFP transgene expression was initiated 24 h later with the addition of 1  $\mu$ g/mL of dox to the culture media. Cells were incubated within the Incucyte Zoom 2000 platform (Essen Biosciences), where continuous imaging (capturing both green and bright field images) was performed. An inclusion formation or growth end point study was performed after 48 h of induction (96 h after cell plating). The Incucyte processing definition of “Inclusions” was designed as follows: parameters, fixed threshold, threshold (GCU) 50; edge split on; edge sensitivity 100; cleanup; hole fill (m<sup>2</sup>): 10; adjust size (pixels); filters; area (m<sup>2</sup>): max 50; mean intensity: min 60; integrated intensity: min 2000. The following processing definition of “Cells” was utilized in determining cell confluence: parameters, segmentation adjustment 0.7; cleanup, all parameters are set to 0; filters, area (m<sup>2</sup>): min 345.00.

**Cell Culture Cotransfection.** The HEK 293T cell line was cultured in DMEM (Invitrogen) with 10% FBS (Invitrogen). Human tau P301S plasmid, cloned in pRK5, was transfected with Lipofectamine 3000 (Invitrogen), and the compounds were added to the cell culture 24 h after transfection. The cells were collected 48 h after compound treatment, and the cell viability was assessed using TypanBlue. Cells were then lysed in 1X TBS with a protease inhibitor (Roche) by sonication (1 min, 30% Amp, 5 s ON –5 s OFF). The lysate was centrifuged at 21,100 g for 10 min at 4 °C. The supernatant (TBS soluble fraction) was transferred into fresh tubes and used for the tau seeding analysis.

**Tau Seeding Assay.** A seeding assay was performed as previously described with modifications.<sup>34,35</sup> TauRD P301S FRET Biosensor cells (ATCC #CRL-3275) were plated at 35,000 cells/well in 130  $\mu$ L of media in a 96-well plate and then incubated at 37 °C overnight. The

next day, cells were transfected with cell lysates (4  $\mu$ g of total protein per well) by using Lipofectamine 2000 and then incubated at 37 °C for 48 h. Cells were harvested by trypsinization. Flow cytometry was conducted with a BD LSRFortessa X-20 instrument with a high-throughput sampler. The BV421 channel (Ex: 405 nm, Em: 450/50) was used to detect CFP, and the BV510 channel (Ex: 405 nm, Em: 525/50 + 505LP) was used to detect the FRET signal, with compensation to remove the CFP spillover into the FRET channel. Data analysis was performed with FlowJo as previously described.<sup>34</sup> Seeding was quantified by the integrated FRET density, defined as the product of the percentage of FRET-positive cells and the median fluorescent intensity (MFI) of FRET-positive cells. Illustrations were made using BioRender.com.

**Solubility Testing.** Kinetic solubilities of compounds 6T and 14T have been achieved at the Medicinal Chemistry Core Facility at Michigan State University. Compounds were solubilized in 10 mM PBS (pH = 7.4) supplemented with 300 mM NaCl and 0.5 mM SDS. This is the buffer used in the ThT assays. The final concentration of DMSO consisted of 1%. Mebendazole was utilized as a control by the core facility. Compounds were tested with a concentration range of 1–100  $\mu$ M. Three replicates were performed. The incubation time consisted of 2 h at 37 °C, and analyses were done with optical density at 620 nm.

**Mouse Microsomal Stability.** The mouse microsomal stability was assessed by the Medicinal Chemistry Core Facility at Michigan State University. Compounds 6T and 14T were tested at a concentration of 3  $\mu$ M. The control consisted of imipramine. Four replicates were analyzed. The buffer consisted of 100 mM phosphate buffer (pH 7.4), 3 mM MgCl<sub>2</sub>, 1 mM NADPH (cofactor), and 1% DMSO. The mouse microsome concentration was 0.25 mg/mL. After 30 min, the stability of each compound was determined using LC–MS/MS. The remaining percentage of compound was reported.

**Animal Studies.** The pharmacokinetic single-dose administration of compounds 6T, 14T, and 19U was performed by Pharmaron using male CD1 mice. Groups consisted of three mice per time point. Single-dose administration of 1 mg/kg was done intravenously. Formulation of the compound consisted of 0.2 mg/mL solution of “10%DMA/90% (20%HP- $\beta$ -CD in water (w/w))”. Blood and brain sampling was performed at 0.083, 0.5, 1, 2, 4, and 8 h. The bioanalytical assay was performed with HPLC–MS/MS.

## ■ ASSOCIATED CONTENT

### Supporting Information

The Supporting Information is available free of charge at <https://pubs.acs.org/doi/10.1021/acscchemneuro.4c00282>.

Additional data pertaining to the characterization of compounds (i.e., <sup>1</sup>H and <sup>13</sup>C NMR characterization and spectra, HPLC purity analysis, and X-ray crystallographic data) (PDF)

## ■ AUTHOR INFORMATION

### Corresponding Author

Jessica S. Fortin – Department of Basic Medical Sciences, College of Veterinary Medicine, Purdue University, West Lafayette, Indiana 47907, United States; [orcid.org/0000-0002-1007-9360](https://orcid.org/0000-0002-1007-9360); Email: [fortinj@purdue.edu](mailto:fortinj@purdue.edu)

### Authors

Susantha K. Ganegamage – Department of Basic Medical Sciences, College of Veterinary Medicine, Purdue University, West Lafayette, Indiana 47907, United States

Taiwo A. Ademoye – Department of Basic Medical Sciences, College of Veterinary Medicine, Purdue University, West Lafayette, Indiana 47907, United States

Henika Patel – Department of Anatomy Cell Biology and Physiology, Indiana University School of Medicine, Indianapolis, Indiana 46202-5114, United States



**Heba Alnakhala** – Ann Romney Center for Neurologic Diseases, Department of Neurology, Brigham and Women's Hospital and Harvard Medical School, Boston, Massachusetts 02115, United States

**Arati Tripathi** – Ann Romney Center for Neurologic Diseases, Department of Neurology, Brigham and Women's Hospital and Harvard Medical School, Boston, Massachusetts 02115, United States

**Cuong Calvin Duc Nguyen** – Department of Chemistry, College of Sciences, Purdue University, West Lafayette, Indiana 47907, United States

**Khai Pham** – Department of Chemistry, College of Sciences, Purdue University, West Lafayette, Indiana 47907, United States

**Germán Plascencia-Villa** – Department of Neuroscience, Developmental and Regenerative Biology, The University of Texas at San Antonio, San Antonio, Texas 78249, United States

**Xiongwei Zhu** – Department of Pathology, Case Western Reserve University, Cleveland, Ohio 44106, United States

**George Perry** – Department of Neuroscience, Developmental and Regenerative Biology, The University of Texas at San Antonio, San Antonio, Texas 78249, United States;

orcid.org/0000-0002-6547-0172

**Shiliang Tian** – Department of Chemistry, College of Sciences, Purdue University, West Lafayette, Indiana 47907, United States; orcid.org/0000-0002-9830-5480

**Ulf Dettmer** – Ann Romney Center for Neurologic Diseases, Department of Neurology, Brigham and Women's Hospital and Harvard Medical School, Boston, Massachusetts 02115, United States

**Cristian Lasagna-Reeves** – Department of Anatomy Cell Biology and Physiology, Indiana University School of Medicine, Indianapolis, Indiana 46202-5114, United States

Complete contact information is available at:

<https://pubs.acs.org/10.1021/acschemneuro.4c00282>

### Author Contributions

S.K.G. and T.A.A. contributed equally to this work. This project was conceived by J.S.F. TEM images were acquired by J.S.F. Synthesis and resynthesis of compounds for quality controls were performed by S.K.G. The ThT assays, cross-linking assays, and data interpretation were performed by T.A.A. The cell culture experiments, statistics, and data interpretation were conducted by H.S.P. (tau biosensor model), C.A.L.-R. (tau biosensor model), H.A. ( $\alpha$ -syn model), A.T. ( $\alpha$ -syn model), and U.D. ( $\alpha$ -syn model). Tau protein procurement and tau ThT assays were performed by C.D.C.N., K.P., and S.T. The procurement of brain samples and extraction of amyloid- $\beta$  plaques were conducted by G.P.-V., X.Z., and G.P. The results were discussed with G.P., U.D., and C.A.L.-R. The manuscript was drafted by S.K.G., T.A.A., and J.S.F. The manuscript was edited by T.A.A., H.S.P., H.A., A.T., and C.D.C.N. All authors contributed to this manuscript and approved the final version of this manuscript.

### Funding

J.S.F. was supported by the National Institutes of Health (NIH) grants (AG070447 and AG071985) and the Pharmaceutical Research and Manufacturers of America Foundation (730313). C.A.L.-R. was supported by the NIH/NIA grant 1R01AG059639, NIH/NINDS grant 1R01NS119280, and the Department of Defense award AZ180006. U.D. was supported

by NIH grants NS121826 and NS099328. G.P.-V. was supported by the Kleberg Foundation, Lowe Foundation, and Alzheimer's Association (AARFD-17-529742).

### Notes

The authors declare no competing financial interest.

### ACKNOWLEDGMENTS

The authors would like to acknowledge the professional services of Alicia Withrow at the Center for Advanced Microscopy at Michigan State University for technical expertise. The authors gratefully acknowledge Pharmaron for the service and expertise on the single-dose administration of compounds as well as Dr. Edmund Ellsworth and Matthew Giletto for the kinetic solubility and mouse microsomal stability data obtained at the MSU Medicinal Chemistry Core facility.

### ABBREVIATIONS

A $\beta$ , amyloid- $\beta$ ; AChE, acetylcholinesterase; AD, Alzheimer's disease; ADME, absorption, distribution, metabolism, and excretion; BACE,  $\beta$ -secretase; CD, circular dichroism; DLB, dementia with Lewy bodies; dox, doxycycline; DTT, dithiothreitol; NFTs, neurofibrillary tangles; MAPT, microtubule-associated protein tau; PD, Parkinson's disease; PK, pharmacokinetics; PICUP, photoinduced cross-linking of unmodified proteins; SEM, standard error of the mean;  $\alpha$ -syn,  $\alpha$ -synuclein; TEM, transmission electron microscopy; ThT, thioflavin T

### REFERENCES

- (1) Knopman, D. S.; Amieva, H.; Petersen, R. C.; Chetelat, G.; Holtzman, D. M.; Hyman, B. T.; Nixon, R. A.; Jones, D. T. Alzheimer disease. *Nat. Rev. Dis. Primers* **2021**, *7* (1), 33.
- (2) Breijyeh, Z.; Karaman, R. Comprehensive Review on Alzheimer's Disease: Causes and Treatment. *Molecules* **2020**, *25* (24), 5789.
- (3) Brandt, R.; Hundelt, M.; Shahani, N. Tau alteration and neuronal degeneration in tauopathies: mechanisms and models. *Biochim. Biophys. Acta* **2005**, *1739* (2–3), 331–354.
- (4) Mandelkow, E.; von Bergen, M.; Biernat, J.; Mandelkow, E. M. Structural principles of tau and the paired helical filaments of Alzheimer's disease. *Brain Pathol.* **2007**, *17* (1), 83–90.
- (5) Guo, T.; Noble, W.; Hanger, D. P. Roles of tau protein in health and disease. *Acta Neuropathol* **2017**, *133* (5), 665–704.
- (6) Hanes, J.; Zilka, N.; Bartkova, M.; Caletkova, M.; Dobrota, D.; Novak, M. Rat tau proteome consists of six tau isoforms: implication for animal models of human tauopathies. *J. Neurochem.* **2009**, *108* (5), 1167–1176.
- (7) Zhang, Y.; Tian, Q.; Zhang, Q.; Zhou, X.; Liu, S.; Wang, J. Z. Hyperphosphorylation of microtubule-associated tau protein plays dual role in neurodegeneration and neuroprotection. *Pathophysiology* **2009**, *16* (4), 311–316.
- (8) Mohandas, E.; Rajmohan, V.; Raghunath, B. Neurobiology of Alzheimer's disease. *Indian J. Psychiatry* **2009**, *51* (1), 55–61.
- (9) Novak, M.; Zilka, N.; Kovacech, B.; Barath, P.; Kontseikova, E. F3-02-03: Tau truncation: The most productive post-translational modification. *Alzheimer's Dementia, J. Alzheimer's Assoc.* **2012**, *8* (4S), 424.
- (10) Beharry, C.; Cohen, L. S.; Di, J.; Ibrahim, K.; Briffa-Mirabella, S.; Alonso Adel, C. Tau-induced neurodegeneration: mechanisms and targets. *Neurosci. Bull.* **2014**, *30* (2), 346–358.
- (11) Muralidar, S.; Ambi, S. V.; Sekaran, S.; Thirumalai, D.; Palaniappan, B. Role of tau protein in Alzheimer's disease: The prime pathological player. *Int. J. Biol. Macromol.* **2020**, *163*, 1599–1617.
- (12) Hickman, S.; Izzy, S.; Sen, P.; Morsett, L.; El Khoury, J. Microglia in neurodegeneration. *Nat. Neurosci.* **2018**, *21* (10), 1359–1369.
- (13) Liu, M.; Sui, D.; Dexheimer, T.; Hovde, S.; Deng, X.; Wang, K. W.; Lin, H. L.; Chien, H. T.; Kweon, H. K.; Kuo, N. S.



Hyperphosphorylation Renders Tau Prone to Aggregate and to Cause Cell Death. *Mol. Neurobiol.* **2020**, *57* (11), 4704–4719.

(14) Graham, W. V.; Bonito-Oliva, A.; Sakmar, T. P. Update on Alzheimer's Disease Therapy and Prevention Strategies. *Annu. Rev. Med.* **2017**, *68*, 413–430.

(15) Osborne, O. M.; Naranjo, O.; Heckmann, B. L.; Dykxhoorn, D.; Toborek, M. Anti-amyloid: An antibody to cure Alzheimer's or an attitude. *iScience* **2023**, *26* (8), No. 107461.

(16) del Ser, T.; Steinwachs, K. C.; Gertz, H. J.; Andres, M. V.; Gomez-Carrillo, B.; Medina, M.; Vericat, J. A.; Redondo, P.; Fleet, D.; Leon, T. Treatment of Alzheimer's disease with the GSK-3 inhibitor tideglusib: a pilot study. *J. Alzheimers Dis.* **2013**, *33* (1), 205–215.

(17) Salloway, S.; Sperling, R.; Fox, N. C.; Blennow, K.; Klunk, W.; Raskind, M.; Sabbagh, M.; Honig, L. S.; Porsteinsson, A. P.; Ferris, S. Two phase 3 trials of bapineuzumab in mild-to-moderate Alzheimer's disease. *N. Engl. J. Med.* **2014**, *370* (4), 322–333.

(18) Fortin, J. S.; Shimanaka, K.; Saraswati, A. P.; Liu, M.; Wang, K. W.; Hagar, H. T.; Maity, S.; Ganegamage, S. K.; Ellsworth, E.; Counts, S. E. Anti-fibrillization effects of sulfonamide derivatives on alpha-synuclein and hyperphosphorylated tau isoform 1N4R. *J. Mol. Struct.* **2022**, *1267*, No. 133574.

(19) Fortin, J. S.; Benoit-Biancamano, M. O.; C-Gaudreault, R. Discovery of ethyl urea derivatives as inhibitors of islet amyloid polypeptide fibrillization and cytotoxicity. *Can. J. Physiol. Pharmacol.* **2016**, *94* (3), 341–346.

(20) Maity, S.; Shimanaka, K.; Rivet, L. N.; O'Dell, M.; Rashid, A. M.; Isa, N. B. M.; Kepczynski, R. S.; Dettmer, U.; Borhan, B.; Fortin, J. S. In vitro characterization of urea derivatives to inhibit alpha-synuclein early-stage aggregation. *J. Mol. Struct.* **2022**, *1249*, No. 131569.

(21) Elbatrawy, A. A.; Ademoye, T. A.; Alnakhala, H.; Tripathi, A.; Zami, A.; Ostafe, R.; Dettmer, U.; Fortin, J. S. Discovery of small molecule benzothiazole and indole derivatives tackling tau 2N4R and alpha-synuclein fibrils. *Bioorg. Med. Chem.* **2024**, *100*, No. 117613.

(22) Ramirez, E.; Ganegamage, S. K.; Min, S.; Patel, H.; Ogunware, A.; Plascencia-Villa, G.; Alnakhala, H.; Shimanaka, K.; Tripathi, A.; Wang, K. W.; et al. Evaluation of N- and O-Linked Indole Triazines for a Dual Effect on alpha-Synuclein and Tau Aggregation. *ACS Chem. Neurosci.* **2023**, *14* (21), 3913–3927.

(23) Ramirez, E.; Min, S.; Ganegamage, S. K.; Shimanaka, K.; Sosa, M. G.; Dettmer, U.; Rochet, J. C.; Fortin, J. S. Discovery of 4-aminoindole carboxamide derivatives to curtail alpha-synuclein and tau isoform 2N4R oligomer formation. *Results Chem.* **2023**, *5*, No. 100938.

(24) Moreno-Gonzalez, I.; Soto, C. Misfolded protein aggregates: mechanisms, structures and potential for disease transmission. *Semin. Cell Dev. Biol.* **2011**, *22* (5), 482–487.

(25) Dettmer, U.; Ramalingam, N.; von Saucken, V. E.; Kim, T. E.; Newman, A. J.; Terry-Kantor, E.; Nuber, S.; Ericsson, M.; Fanning, S.; Bartels, T. Loss of native alpha-synuclein multimerization by strategically mutating its amphipathic helix causes abnormal vesicle interactions in neuronal cells. *Hum. Mol. Genet.* **2017**, *26* (18), 3466–3481.

(26) Dettmer, U.; Newman, A. J.; Soldner, F.; Luth, E. S.; Kim, N. C.; von Saucken, V. E.; Sanderson, J. B.; Jaenisch, R.; Bartels, T.; Selkoe, D. Corrigendum: Parkinson-causing alpha-synuclein missense mutations shift native tetramers to monomers as a mechanism for disease initiation. *Nat. Commun.* **2015**, *6*, 8008.

(27) Dettmer, U.; Newman, A. J.; Soldner, F.; Luth, E. S.; Kim, N. C.; von Saucken, V. E.; Sanderson, J. B.; Jaenisch, R.; Bartels, T.; Selkoe, D. Parkinson-causing alpha-synuclein missense mutations shift native tetramers to monomers as a mechanism for disease initiation. *Nat. Commun.* **2015**, *6*, 7314.

(28) Terry-Kantor, E.; Tripathi, A.; Imberdis, T.; LaVoie, Z. M.; Ho, G. P. H.; Selkoe, D.; Fanning, S.; Ramalingam, N.; Dettmer, U. Rapid Alpha-Synuclein Toxicity in a Neural Cell Model and Its Rescue by a Stearoyl-CoA Desaturase Inhibitor. *Int. J. Mol. Sci.* **2020**, *21* (15), 5193.

(29) Imberdis, T.; Negri, J.; Ramalingam, N.; Terry-Kantor, E.; Ho, G. P. H.; Fanning, S.; Stirtz, G.; Kim, T. E.; Levy, O. A.; Young-Pearse, T. L. Cell models of lipid-rich alpha-synuclein aggregation validate known

modifiers of alpha-synuclein biology and identify stearyl-CoA desaturase. *Proc. Natl. Acad. Sci. U. S. A.* **2019**, *116* (41), 20760–20769.

(30) Ramirez, E.; Ganegamage, S. K.; Elbatrawy, A. A.; Alnakhala, H.; Shimanaka, K.; Tripathi, A.; Min, S.; Rochet, J. C.; Dettmer, U.; Fortin, J. S. 5-Nitro-1,2-benzothiazol-3-amine and N-Ethyl-1-[(ethylcarbamoyl)(5-nitro-1,2-benzothiazol-3-yl)amino]formamide Modulate alpha-Synuclein and Tau Aggregation. *ACS Omega* **2023**, *8* (22), 20102–20115.

(31) Dregni, A. J.; Wang, H. K.; Wu, H.; Duan, P.; Jin, J.; DeGrado, W. F.; Hong, M. Inclusion of the C-Terminal Domain in the beta-Sheet Core of Heparin-Fibrillized Three-Repeat Tau Protein Revealed by Solid-State Nuclear Magnetic Resonance Spectroscopy. *J. Am. Chem. Soc.* **2021**, *143* (20), 7839–7851.

(32) Barghorn, S.; Biernat, J.; Mandelkow, E. Purification of recombinant tau protein and preparation of Alzheimer-paired helical filaments in vitro. *Methods Mol. Biol.* **2005**, *299*, 35–51.

(33) Wu, L.; Wang, Z.; Lad, S.; Gilyazova, N.; Dougharty, D. T.; Marcus, M.; Henderson, F.; Ray, W. K.; Siedlak, S.; Li, J. Selective Detection of Misfolded Tau From Postmortem Alzheimer's Disease Brains. *Front. Aging Neurosci.* **2022**, *14*, No. 945875.

(34) Martinez, P.; Patel, H.; You, Y.; Jury, N.; Perkins, A.; Lee-Gosselin, A.; Taylor, X.; You, Y.; Viana Di Prisco, G.; Huang, X. Bassoon contributes to tau-seed propagation and neurotoxicity. *Nat. Neurosci.* **2022**, *25* (12), 1597–1607.

(35) Patel, H.; Martinez, P.; Perkins, A.; Taylor, X.; Jury, N.; McKinzie, D.; Lasagna-Reeves, C. A. Pathological tau and reactive astrogliosis are associated with distinct functional deficits in a mouse model of tauopathy. *Neurobiol. Aging* **2022**, *109*, 52–63.